NASA Tech Briefs

National Aeronautics and Space Administration

97-11

November 1997

INTRODUCTION

Tech Briefs are short announcements of new technology derived from the research and development activities of the National Aeronautics and Space Administration. These Briefs emphasize information considered likely to be transferable across industrial, regional, or disciplinary lines and are issued to encourage commercial application.

Availability of NASA Tech Briefs and TSP's

Distribution of NASA Tech Briefs, a monthly periodical publication, is limited to engineers in U.S. industry and to other domestic technology transfer agents. Requests for individual Tech Briefs or for Technical Support Packages (TSP's) announced herein should be addressed to

NASA Center for AeroSpace Information
Technology Transfer Office
800 Elkridge Landing Rd.
Linthicum Heights, MD 21090-2934
Telephone No. (301) 621-0245

Please reference the three-letter, five-digit control number located at the end of each Tech Brief. Information on NASA's Technology Utilization Program, its documents, and services is also available at the same facility.

Technology Utilization Officers and Patent Counsels are located at NASA field installations to provide technology-transfer access to industrial users. Inquiries can be made by writing to NASA field installations listed below.

Technology Utilization Officers and Patent Counsels

Ames Research Center
Technology Utilization Officer
Mail Code 223-3
Moffett Field, CA 94035

Patent Counsel
Mail Code 200-11
Moffett Field, CA 94035

Goddard Space Flight Center
Technology Utilization Officer
Mail Code 702-1
Greenbelt, MD 20771

Patent Counsel
Mail Code 204
Greenbelt, MD 20771

Lyndon B. Johnson Space Center
Technology Utilization Officer
Mail Code IC-4
Houston, TX 77058

Patent Counsel
Mail Code AL3
Houston, TX 77058

John F. Kennedy Space Center
Technology Utilization Officer
Mail Stop PT-PMO-A
Kennedy Space Center, FL 32899

Patent Counsel
Mail Code PT-PAT
Kennedy Space Center, FL 32899

Langley Research Center
Technology Utilization Officer
Mail Stop 143
Hampton, VA 23665

Patent Counsel
Mail Code 279
Hampton, VA 23665

Lewis Research Center
Technology Utilization Officer
Mail Stop 7-3
21000 Brookpark Road
Cleveland, OH 44135

Patent Counsel
Mail Code LE-LAW
21000 Brookpark Road
Cleveland, OH 44135

Jet Propulsion Laboratory
Technology Utilization Officer
Mail Stop 156-211
4800 Oak Grove Drive
Pasadena, CA 91109

NASA Resident Office-JPL
Technology Utilization Officer
Mail Stop 180-801
4800 Oak Grove Drive
Pasadena, CA 91109

Patent Counsel
Mail Code 180-801
4800 Oak Grove Drive
Pasadena, CA 91109

George C. Marshall Space Flight Center
Technology Utilization Officer
Code AT01
Marshall Space Flight Center, AL 35812

Patent Counsel
Mail Code CC01
Marshall Space Flight Center, AL 35812

John C. Stennis Space Center
Technology Utilization Officer
Code HA-30
Stennis Space Center, MS 39529

NASA Headquarters
Technology Utilization Officer
Code CU
Washington, DC 20546

Assistant General Counsel for Patent Matters
Code GP
Washington, DC 20546

Dryden Flight Research Center
Technology Utilization Officer
M/S D21-31
Bldg. 4832 Whse 7
Lilly Dr.
Edwards, CA 93523

NASA TechBriefs

November 1997
97-11

National Aeronautics and Space Administration

BLANK PAGE

Electronic Components and Circuits

Hardware, Techniques, and Processes

BLANK PAGE

Signal-Decay Technique for Determining Qs of Power Inductors

There are no switches in the test inductor/capacitor loops.

Lewis Research Center, Cleveland, Ohio

An improved resonant-signal-decay technique has been devised for measuring electrical losses in quasi-linear inductors of the type that are used in modern electronic power-supply circuits and that are typically operated at frequencies up to about 100 kHz. The basic resonant-signal-decay technique has been used since the early years of electronics. The essence of the basic technique is to connect an inductor with a low-loss capacitor in a simple loop resonant circuit, apply a one-shot pulsed signal to excite oscillations at the resonance frequency, and measure the rate of decay of the signal to determine the electrical loss in the circuit at the resonance frequency. [Customarily, electrical loss is expressed in terms of a resonance quality factor, $Q = \pi f/\alpha$, where f = the resonance frequency and α = the rate (reciprocal of characteristic time) of exponential decay.] The outstanding feature of the present improved resonant-signal-decay technique is that unlike in older such techniques, extraneous switching electrical losses are minimized by avoiding the connection of any switches in series with the inductor and capacitor in the loop. Electronic switches in the form of metal oxide/semiconductor field-effect transistors (MOSFETs) are still present, but the circuit is configured and operated in such a way that the losses introduced by the MOSFET switches are negligible in comparison with those introduced by the inductor and capacitor.

Figure 1 illustrates the circuit used in the improved technique. The terminals of a low-loss, polypropylene-film-dielectric capacitor are connected directly to the terminals of the inductor to be tested. Excitation from an ac source is supplied in a parallel-resonant configuration via a back-to-back pair of high-voltage power MOSFETs. Though it is not strictly necessary to do so, it is desirable to set the excitation frequency at or near the resonance frequency of the inductor-and-capacitor loop. The excitation is applied during a brief pulse, using the same trigger pulse to turn both the MOSFETs and the ac source on momentarily. (It is necessary to turn the ac source off after applying the excitation to prevent spurious coupling of the excitatory signal through the internal capacitances of the MOSFETs.) At resonance frequencies ≤100 kHz, the radiative losses, like the losses in the MOSFETs, are much smaller than are the losses in the inductor and capacitor.

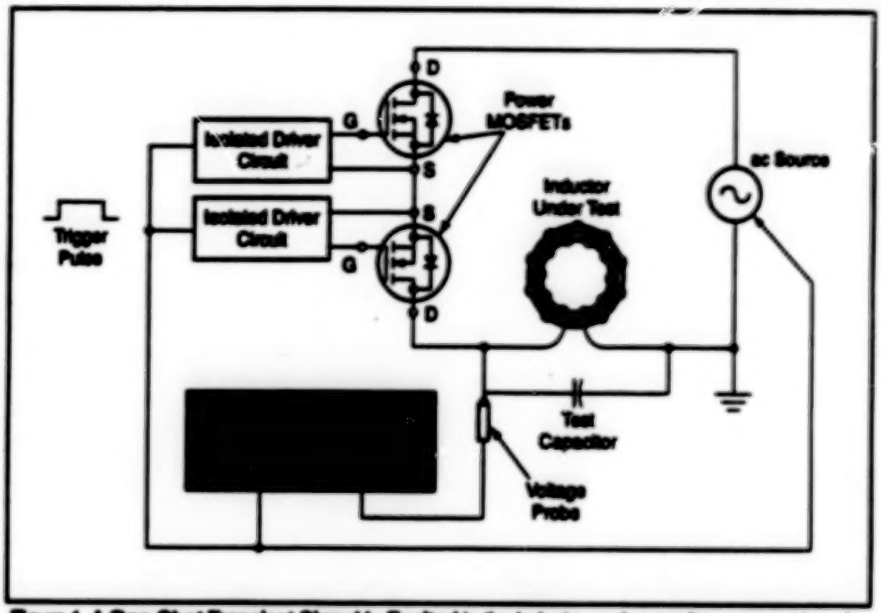

Figure 1. A One-Shot Transient Signal Is Excited in the inductor-and-capacitor resonant loop by momentary application of an ac signal during a trigger pulse. The digital oscilloscope records the resulting decaying oscillation.

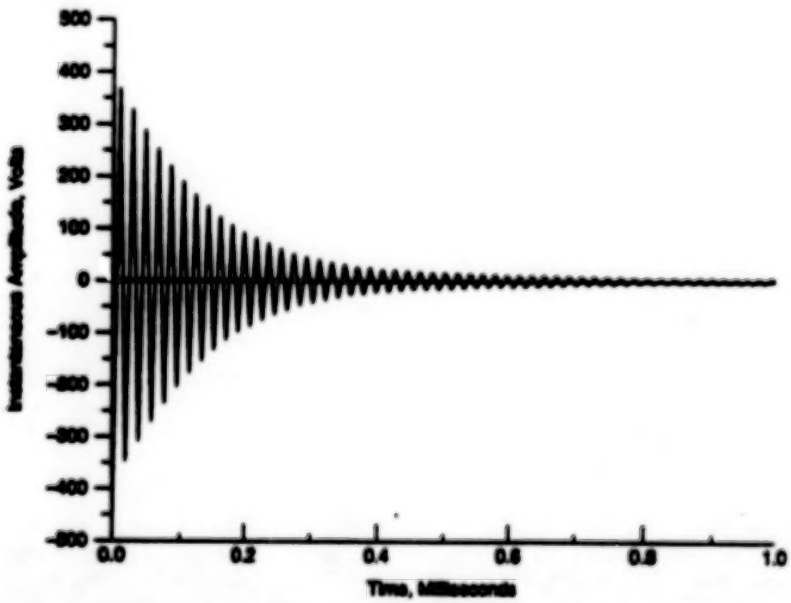

Figure 2. This Decaying Oscillation was recorded in the circuit of Figure 1 with a test capacitor of 0.22 μF and a ferrite-core inductor of 35.6 μH.

The trigger pulse is also used to trigger a digitizing oscilloscope, which measures the voltage waveform to capture the decaying oscillation (see Figure 2). The Q of the circuit is then computed by means of a polynomial fit to the peaks of the decaying voltage waveform; experiments have shown that 10-degree polynomials give good fits in most cases.

This work was done by Janis M. Niedra and Scott S. Gerber of NYMA, Inc., for Lewis Research Center. Further information is contained in a TSP [see page 1].

Inquiries concerning rights for the commercial use of this invention should be addressed to NASA Lewis Research Center, Commercial Technology Office, Attn: Tech Brief Patent Status, Mail Stop 7–3, 21000 Brookpark Road, Cleveland, Ohio 44135. Refer to LEW-16444.

Bidirectional Electronic Circuit Breaker

Adequate precision is achieved with a relatively simple circuit.

Lewis Research Center, Cleveland, Ohio

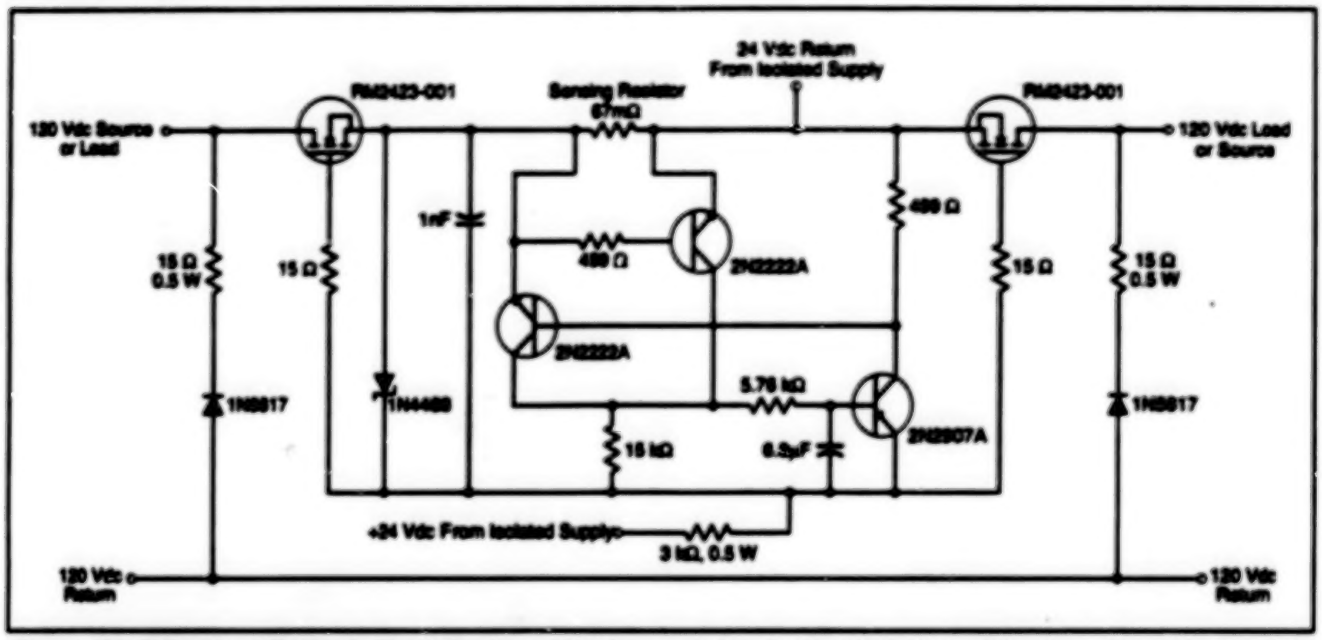

Figure 1. This Bidirectional Electronic Circuit Breaker contains fewer parts than do other electronic circuit breakers, yet is precise enough for its original purpose.

An electronic circuit breaker is designed to trip at a nominal direct current of 5.6 A (or more, depending on temperature). The current can be of either polarity. Originally designed for use in a cross-feed link between two loads powered by a redundant pair of power sources, this circuit breaker could also be used in other applications in which protection against dc overcurrent of either polarity is needed.

Fuses were rejected for use in the original application because the overcurrent conditions under which they trip cannot be established with sufficient precision. Very precise electronic circuit breakers containing operational amplifiers, comparators, and other integrated circuits were also rejected because they were judged to be too complex for that application. The present bidirectional electronic circuit breaker was designed as a compromise between the two extremes, providing adequate precision with minimal complexity and a relatively small number of parts.

The bidirectional circuit breaker (see Figure 1) requires an isolated 24-Vdc power supply. During normal operation, the main load current is conducted through the two RM2423-001 metal oxide/semiconductor field-effect transistors (MOSFETs) and through the sensing resistor. The value (67 mΩ) of this resistor is chosen so that when the magnitude of the load current equals or exceeds the desired trip level, the voltage across this resistor equals or exceeds the turn-on threshold base-to-emitter voltage of one of the 2N2222A npn transistors.

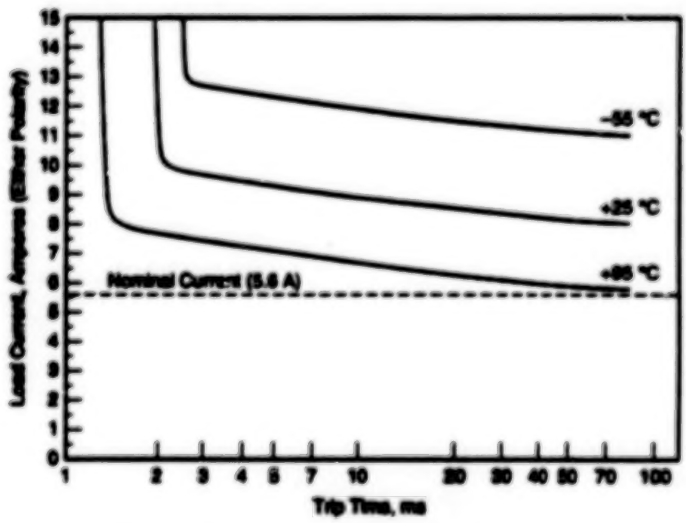

Figure 2. The Circuit Breaker Is Tripped into turn-off when the point that represents its operating condition lies on or above the curve for the operating temperature. Note that the circuit is not tripped by large current pulses shorter than about 1 ms.

The turning on of either 2N2222A npn transistor causes the turn-on of the 2N2907A pnp transistor, which is the active element of a latching circuit. When thus activated, the latching circuit lowers the voltages on the MOSFET gates below their conducting thresholds. Thus, the MOSFETs are turned off, interrupting the path for the load current.

The latching circuit includes a resistor/capacitor delay circuit that makes the circuit breaker insensitive to a current surge shorter than about 1 ms (see Figure 2). Once the circuit breaker has been tripped by overcurrent, and until it is reset, the latching circuit holds it in the "off" condition. Reset is accomplished by turning

off, then turning on the isolated 24-Vdc power supply.

This work was done by Tomasz Kachelski of Rockwell International Corp. for Lewis Research Center. Further information is contained in a TSP [see page 1].

Inquiries concerning rights for the commercial use of this invention should be addressed to the Patent Counsel, Lewis Research Center [see page 1]. Refer to LEW-16027.

Slotted Carbon/Carbon Grids for Ion Accelerators

These grids offer potential advantages over metal grids made with wires or circular holes.

NASA's Jet Propulsion Laboratory, Pasadena, California

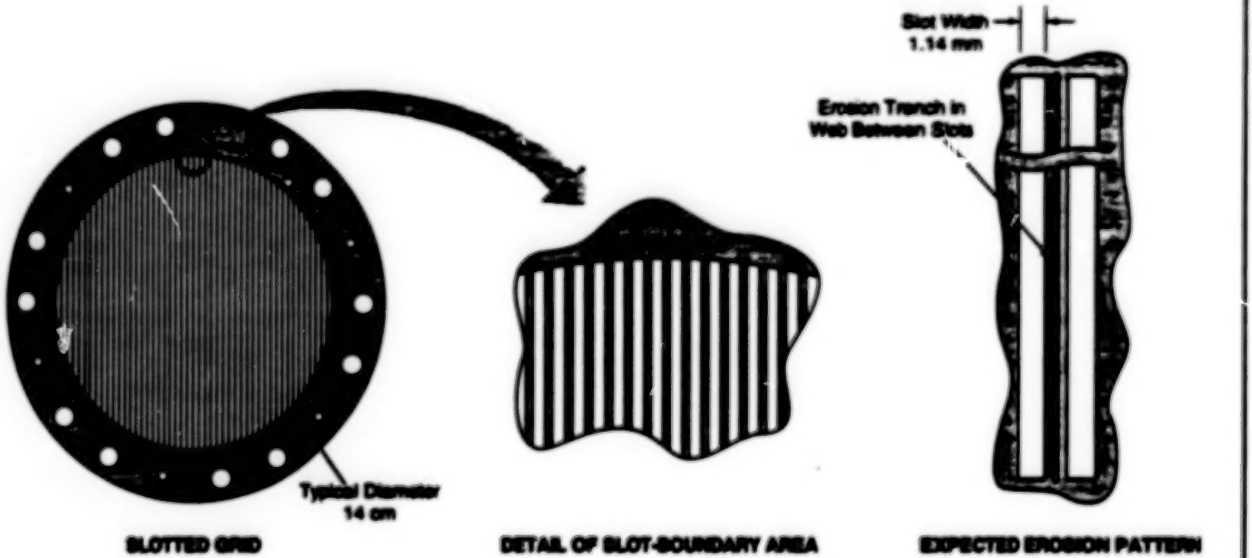

A Slotted Carbon/Carbon Grid could be machined at relatively low cost. The grid would erode along the center lines of the webs between the slots; this erosion pattern would delay structural failure.

Ion-accelerator grids made by machining long parallel slots into solid pieces of carbon/carbon composite material have been proposed to replace ion-accelerator grids made by chemically etching circular holes in hexagonal patterns in molybdenum sheets. The proposed slotted carbon/carbon grids would resemble the metal wire grids used in the first ion engine built in 1960, but would offer advantages over both the early wire grids and the chemically-etched-molybdenum-sheet grids now in use.

Several previous articles in *NASA Tech Briefs* have discussed various aspects of replacing metal ion-accelerator grids with carbon/carbon grids. Briefly, the potential advantages of carbon/carbon grids over metal grids include (1) a lower rate of erosion of carbon/carbon by charge-exchange ions; (2) low or negative coefficient of thermal expansion of carbon/carbon, with consequent reduction or elimination of thermal distortion at high operating temperatures; and (3) greater rigidity of carbon/carbon grids, with consequent greater ability to resist electrostatic deflection and maintain required precise geometry at high applied voltages.

The present concept of long, parallel slots in carbon/carbon sheets is an extension of the concept described in "Ion-Accelerator Grids With Elongated Holes" (NPO-19336), *NASA Tech Briefs*, Vol. 20, No. 1, (January 1996), page 34. One reason for choosing long, parallel slots instead of patterns of circular or elongated holes is that grids containing long, parallel slots are expected to endure erosion better. A hexagonal erosion pattern is formed by charge-exchange ions on a molybdenum ion-accelerator grid with a conventional hexagonal pattern of round holes. Structural failure occurs when the depth of erosion reaches the full thickness of the grid. However, in a slotted carbon/carbon grid (see figure), the erosion pattern is expected to consist of longitudinal trenches centered in the webs between slots. In this case, erosion completely through the thickness would not cause immediate structural failure; rather, it would divide each web into two narrower parallel webs. It has been estimated that a parallel-slot grid would last three times as long as would a round-hole/hexagonal-pattern grid of the same material, taking this factor in combination with the lower rate of erosion of carbon/carbon (expected to be less than 1/6 that of molybdenum), it appears that a slotted carbon/carbon grid should have an operational life 18 times that of a comparable round-hole/hexagonal pattern molybdenum grid.

In fabricating a slotted carbon/carbon grid, the slots would be machined parallel to the majority of carbon fibers in a carbon/carbon sheet. Machining in this pattern would leave a large number of uncut fibers extending across the full diameter of the grid, resulting in a substantial increase in the stiffness of the grid over that of a grid with a hexagonal pattern of circular holes. The cost of machining the grid slots has been estimated to be about 1/6 that of machining grid holes in a hexagonal pattern. The main reason for the decrease in cost is that for a grid of a given size (e.g., a diameter of 14 cm and thickness of 0.5 mm) the number of slots (about 50) would be much smaller than the number of holes (about 4,000).

This work was done by John R. Brophy, D. Kyle Brown, Juergen Mueller, and Charles E. Garner of Caltech for NASA's Jet Propulsion Laboratory. Further information is contained in a TSP [see page 1].
NPO-19679

Electronic Systems

Hardware, Techniques, and Processes

BLANK PAGE

Heterodyne Interferometers for Subpicometer Metrology

Careful design and implementation reduce rms errors.

NASA's Jet Propulsion Laboratory, Pasadena, California

Improved heterodyne interferometric gauges are undergoing development for use in monitoring distances within root-mean-square (rms) errors of the order of a picometer or less. Heretofore, state-of-the-art commercial and custom-made interferometers have been capable of monitoring distances to within rms errors no smaller than about 1 nanometer.

One of the improved gauges, denoted a null-metrology gauge, includes two interferometers with spatially coincident light paths (see Figure 1). The distance to be monitored is also required to be maintained constant to high precision. To maintain constancy, this distance is servoed to the null of one interferometer. The other interferometer is used as a readout device. The use of spatially coincident light paths makes it possible to eliminate the effect of air-density fluctuations, which would otherwise give rise to a minimum achievable rms error of the order of 10 nm.

The single source of light for both interferometers is a frequency-stabilized He/Ne laser. A 45° linear polarizer and a polarizing beam splitter separate the laser beam into two beams with orthogonal polarizations (denoted "S" and "P"). Each of these beams is routed through one of two acousto-optical modulators. A frequency of *f* exists on the radio frequency signal applied to only one of the modulators. A signal with frequencies of *f* + 10 kHz and *f* + 20 kHz is applied to the other modulator. As a result, the photodetector output that sees only the "best" frequencies contains 10-kHz, 20-kHz, and 30-kHz signals. Among these, only 10 kHz and 20 kHz are real signals; 30 kHz is a spurious signal. The modulated beams are recombined by another polarizing beam splitter, then spatially filtered in a pinhole assembly.

By use of another polarizing-beam-splitter-and-polarizer combination, a small part of the recombined beam is diverted to a photodiode denoted the "reference" photodetector. The rest of the recombined beam enters a beam-launching assembly that comprises a polarizing beam splitter and two quarter-wave plates. Half of the recombined beam passes directly through the polarizing beam splitter, then through a 45° polarizer, and strikes another photodiode, which is denoted the "unknown" photodetector. The other half of the recombined beam makes a round trip between two corner-cube reflectors separated by a nominal distance of about 75 cm, then follows along the path of the preceding half of the beam to the unknown photodetector.

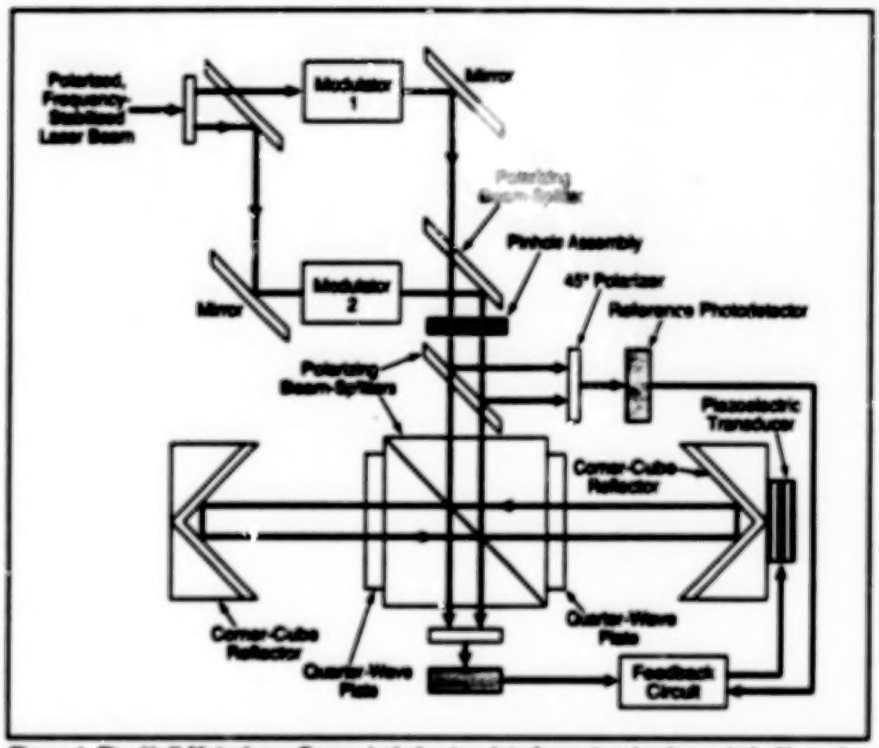

Figure 1. The Null-Metrology Gauge includes two interferometers implemented with modulated, polarized light beams from the same laser propagating along spatially coincident paths.

The outputs of both photodetectors contain signals at frequencies of 10, 20, and 30 kHz. (The two different combinations of modulating frequencies make it possible to distinguish between the two interferometers in subsequent processing of these signals.) For each frequency, the difference between the phases of the signals from the unknown and reference photodetectors is a measure of the distance between the corner-cube reflectors. (This is the distance that one seeks to monitor and maintain constant.)

The signals at the three frequencies are processed by a combination of analog and digital circuitry to obtain, from one interferometer, a digital relative-phase signal and an analog phase-feedback signal that is applied to a piezoelectric transducer to translate one of the corner-cube reflectors to hold the interferometer at null. The signals are also processed to obtain a distance-monitoring relative-phase signal from the other interferometer. During an observation, the digital relative-phase signals from both interferometers are recorded for subsequent analysis.

Another of the improved gauges, denoted a relative-metrology gauge, includes two interferometers with spatially separate light paths (see Figure 2). One interferometer is used to servo the distance between two corner-cube reflectors to a slowly varying separation, while the other interferometer is used as a readout device. Unlike in the null-metrology gauge, the spatial separation of interferometers makes it unnecessary to use different combinations of signal frequencies to distinguish between the two interferometers; accordingly, each acousto-optical modulator is driven at a single frequency that differs by 10 kHz from the frequency applied to the other modulator.

The relative-metrology gauge is designed to classify and eliminate various systematic errors that are not present in a null-metrology gauge. The principal systematic errors are (1) periodic errors associated with polarization leakage in imperfect optical components and (2)

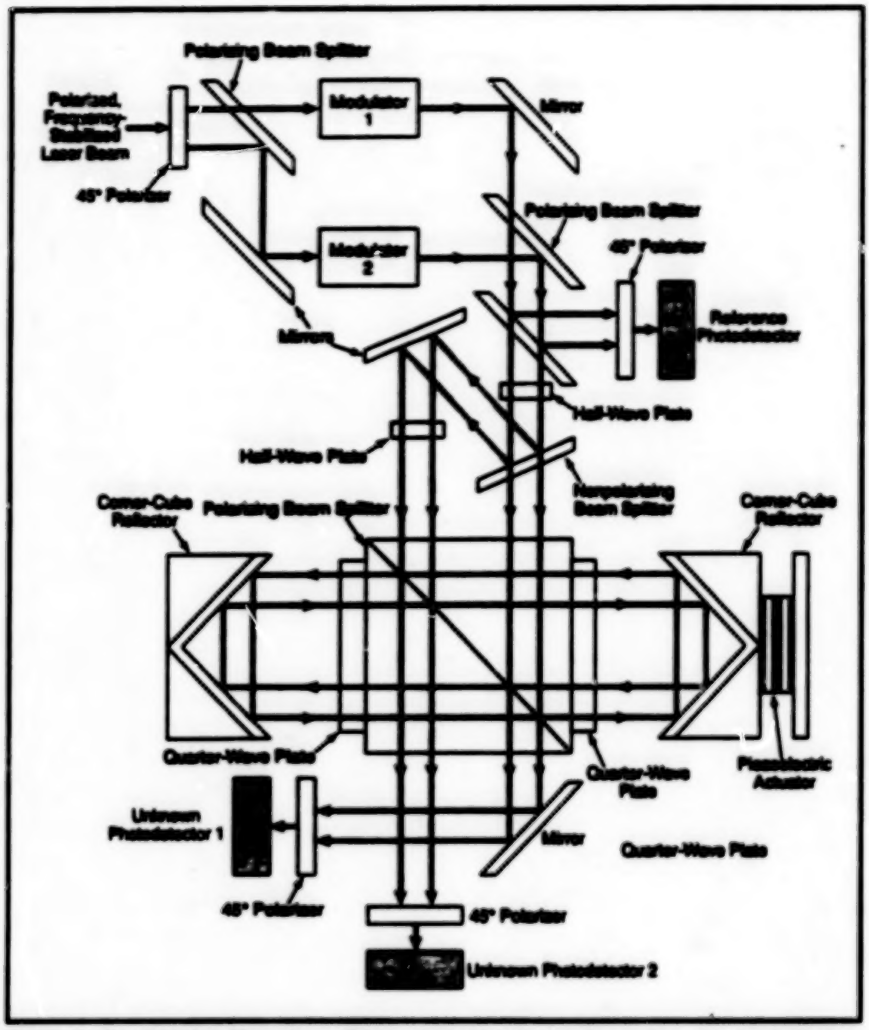

Figure 2. The Relative-Metrology Gauge includes two interferometers also implemented with polarized, modulated light beams from the same laser, but in this case, the beams propagate along separate paths.

errors associated with temperature gradients. The temperature-gradient errors are minimized by actively stabilizing the temperatures of optical components and performing measurements quickly, before significant drift can accumulate. The polarization-leakage errors are eliminated by a method called "cyclic averaging," which involves either using a piezoelectric transducer to modulate the distance to be measured or sweeping the laser frequency at a rate that is fast in comparison with the changes in distance being measured. The amplitude of the modulation is chosen to be several wavelengths of light. The output of each interferometer is recorded at a rate sufficient to guarantee many readings during one wavelength of motion due to modulation. The true output of the interferometers at the center of modulation is computed to be the average over one exact wavelength around the center of modulation.

The null- and relative-metrology gauges have exhibited unprecedented precision: In tests, the null-metrology gauge performed with rms errors as low as 0.6 pm over observation times of 2,500 s. In other tests, the relative-metrology gauge operating in a vacuum exhibited rms errors as low as 0.13 pm over observation times of a few minutes.

This work was done by Yekta Gursel of Caltech for NASA's Jet Propulsion Laboratory. Further information is contained in a TSP [see page 1].
NPO-20046

Programmable Switch Assembly for Aircraft Systems

Feedback from controlled equipment results in visual indications of malfunctions.

Dryden Flight Research Center, Edwards, California

An autonomous programmable switch assembly (PSA) has been developed for use in the Research Instrumentation branch of NASA Dryden Flight Research Center to address the complex and varying system-control requirements of research aircraft. The PSA is now in flight-operational status in the NASA SR-71 airplane. The PSA includes four cockpit switches (see Figure 1) coupled to a microcontroller and to a relay board (see Figure 2) designed at Dryden Flight Research Center.

One of the advantages of the PSA is that it provides engineers with the capability to reduce as many as 16 individual cockpit switches and indicators to one. In addition, the PSA provides feedback from controlled equipment, indicating the current state of the equipment. Individual changes in an installed control system consist of changes in software and wiring and are nominally accomplished within one-day turnaround times. The realm of applicability of PSA extends beyond research aircraft in that it provides capabilities for easily controlling other systems with feedback requirements.

The PSA includes three main components: the Viviun 5000 (or equivalent) electro-optical display system, a Tattletale model 7 (or equivalent) computer (the microcontroller), and the relay boards mentioned above. The display system includes four 1-by-1.5-in. (2.5-by-3.8-cm) programmable multifunction pushbuttons (PMPs), which are the cockpit switches mentioned above. Each PMP contains 560 light-emitting-diode (LED) elements that are readable in sunlight. The display system also includes a refresh processor unit (RPU), which serves as an interface between the PMPs and the microcontroller. The RPU accepts data that are in RS-232 ASCII format and that include specified sequences of control characters that provide for textual and graphical displays on the PMPs. The capabilities for controlling the display include the ability to make one or all of the PMPs blink, turn all the pixels on, perform a self-test, clear the display, and select any of 35 levels of luminance.

The microcontroller is a high-performance data logger based on the Motorola 68332 (or equivalent) microprocessor. It is programmable in ANSI C; the program can be written on a personal computer and downloaded to a nonvolatile flash electrically erasable programmable read-only

memory (EEPROM) in the microcontroller.

The microcontroller includes 12 general-purpose input/output (I/O) pins, nine of which are used for feedback from the relay boards. The feedback informs the microcontroller that a switch action has occurred. If there is a malfunction, the microcontroller causes the display on the appropriate switch to blink. The output from the microcontroller to the relay boards is in the form of eight-bit addresses transmitted via output pins of a time-processor unit in the microprocessor. These addresses are decoded by circuits on the relay boards and used to actuate the appropriate relays. The downloading of software from the personal computer is accomplished via a serial port by use of a terminal program.

Interface boards for the microcontroller were also developed at Dryden Flight Research Center and include the following: a basic operations board, a buffer board, and a serial I/O board. The boards serve as the interfaces among the RPU board, the relay boards, and the personal computer (which is used for monitoring activity as well as programming).

Each relay board holds a dc-to-dc power converter, eight relays, and an address-decoding circuit. The dc-to-dc converter supplies power at a potential of 5 V for the relay outputs and the address decoder. The relays are of the nonlatching, double-throw type. One of two outputs goes to the circuit or relay of interest; the other output provides feedback to the microcontroller. This is the feedback, mentioned previously, that results in a change in the switch display. If the change is intentional and is the result of pressing a switch, then the face of the switch displays the expected result. If the feedback is triggered by a failure, then the switch display blinks as mentioned before and indicates "FAIL" on the display.

This work was done by Michael Toberman of **Dryden Flight Research Center.** *Further information is contained in a TSP [see page 1].*

DFRC-97-04

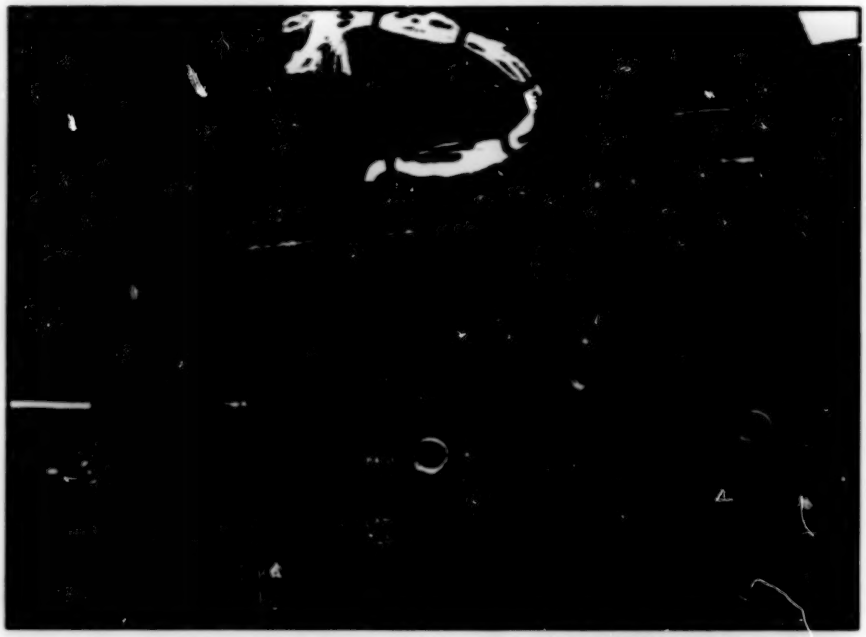

Figure 1. Four Programmable Switches equipped with LED displays are installed in the SR-71 cockpit.

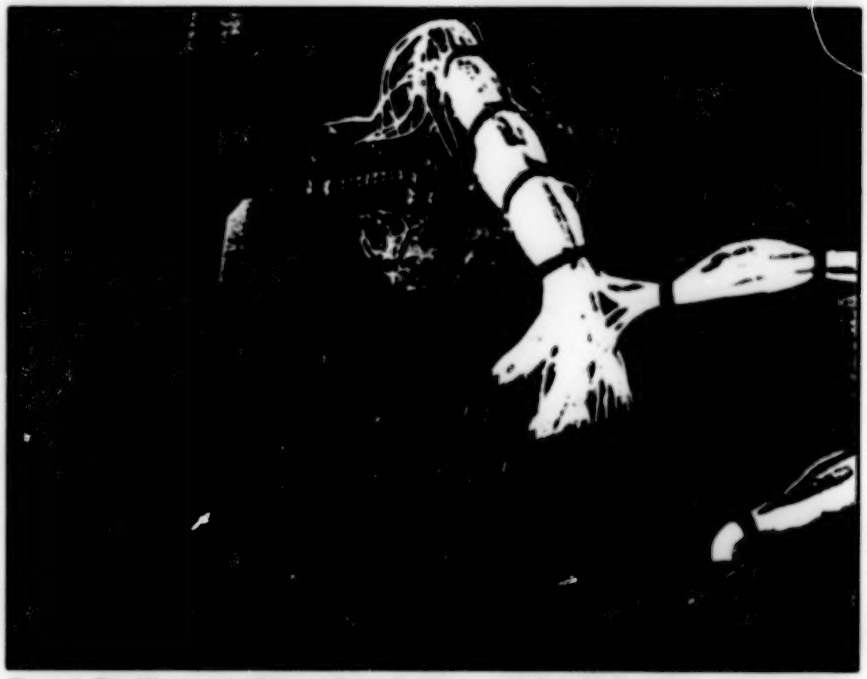

Figure 2. The Microcontroller and Relay Board are installed together as a set in the SR-71 cockpit.

Stabilizing a Photonic Heterodyne Microwave Oscillator

A frequency discriminator built around a fiber-optic delay line would be used.

NASA's Jet Propulsion Laboratory, Pasadena, California

In a proposed scheme for generating a microwave or millimeter-wave signal as a heterodyne product of the outputs of two narrow-band lasers, the frequency of the signal would be stabilized by using a frequency discriminator based on a fiber-optic delay line to stabilize the frequency of one of the lasers. This scheme can be regarded as an extension of the use of such a frequency discriminator to stabilize an electronic microwave oscillator, as reported in "Fiber-Optic Discriminator Stabilizes Microwave Oscillator" (NPO-18375), *Laser Tech Briefs*, Vol. 1, No. 1 (September, 1993), page 24.

Despite their potential utility and potential commercial value, photonic heterodyne microwave oscillators have not yet come into widespread use because of excessive instability of frequency. The proposed scheme would overcome this limitation; theoretically it offers the potential to yield frequency stability equal to or better

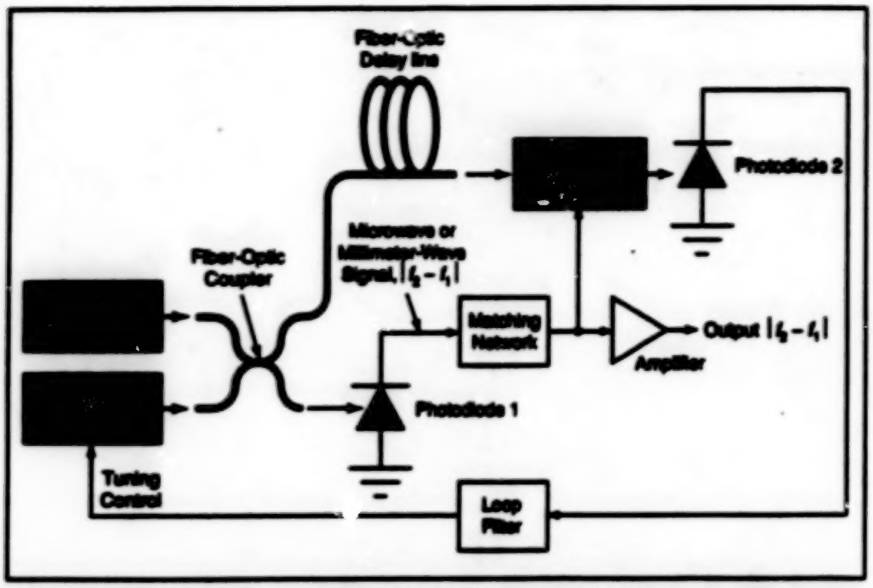

A Frequency Discriminator and Feedback Control Loop based on a fiber-optic delay line and an electro-optical modulator would stabilize the frequency of a photonic heterodyne microwave or millimeter-wave oscillator.

than that of currently available electronic microwave sources.

As shown in the figure, the outputs of the two lasers would be directed into optical fibers and heterodyned by use of a fiber-optic coupler and photodiodes. The coupler would produce two light-signal outputs. The output from one branch of the fiber-optic coupler would go directly to photodiode 1, which would perform the customary detection-and-mixing function, so that one of the components of the electrical output of photodiode 1 would be the desired microwave or millimeter-wave radio signal with a frequency equal to the difference between the two laser frequencies. This signal would be coupled through a matching network to the electrical input terminals of an electro-optical modulator. This signal would also be fed to an amplifier, and the amplified signal would constitute the desired output.

The other branch of the fiber-optic coupler would continue into a fiber-optic delay line to the optical input port of the electro-optical modulator. The output of the electro-optical modulator would be fed to photodiode 2. Provided that the length of the delay line was chosen to obtain phase quadrature at the radio frequency, the heterodyne action in the electro-optical modulator and photodiode 2 would cause the baseband component of the output of photodiode 2 to be proportional to the fluctuation of the phase and frequency of the radio signal during the delay. This baseband output would serve as a feedback error signal to tune one of the lasers to reduce the error and thus stabilize the output frequency.

This work was done by Ronald T. Logan, Jr., of Caltech for NASA's Jet Propulsion Laboratory. Further information is contained in a TSP [see page 1].

In accordance with Public Law 96-517, the contractor has elected to retain title to this invention. Inquiries concerning rights for its commercial use should be addressed to

Larry Gilbert, Director
Technology Transfer
California Institute of Technology
Mail Code 315-6
Pasadena, CA 91125
(818) 395-3288

Refer to NPO-19439, volume and number of this NASA Tech Briefs *issue, and the page number.*

Continuous Measurement of Delay Bias in a GPS Receiver

Occasional manual calibration, which is disruptive, is replaced by a continuous automated process.

NASA's Jet Propulsion Laboratory, Pasadena, California

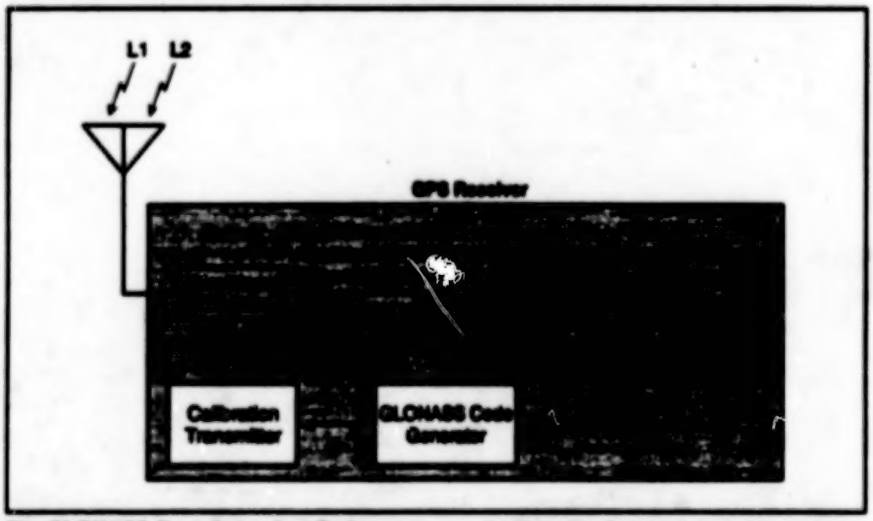

The GLONASS Pseudorandom Code serves as a signal marker that can be used to measure the delay bias between the L1 and L2 signals.

A technique has been devised to enable a Global Positioning System (GPS) receiver to automatically and continuously measure its own delay bias. "Delay bias" signifies the difference between the times of propagation, through the receiver, of the information modulated onto two L-band signals. These signals are called "L1" (with a carrier frequency of 1.57542 GHz) and "L2" (with a carrier frequency of 1.2276 GHz) and are phase-modulated with pseudorandom-noise codes that contain GPS information. The L1 and L2 signals are fed through a signal-processing chain that includes common parts as well as parallel but separate L1 and L2 parts. Delay bias arises from (1) differences between times consumed in processing in the separate L1 and L2 parts

and (2) frequency dispersion in the common parts.

It is necessary to measure and correct for delay biases in order to be able to measure densities of electrons integrated along GPS-signal-propagation-paths through the ionosphere. In turn, the electron-density information can be used to increase the accuracy of GPS mapping and related scientific functions. An older technique for measuring delay biases involves occasional manual calibration, which disrupts what would otherwise be continuous GPS-data-taking operations.

The technique for continuous automated calibration involves the use of a calibration transmitter that phase-modulates a pseudorandom code onto the L1 and L2 carriers (see figure). This code is used in the Russian Global Navigation Satellite System (GLONASS) and is similar to, but distinct from, the GPS codes. At the point of introduction into the L1/L2 signal-processing chain, there is negligible differential delay between the L1 and L2 versions of this signal. This point is as far as possible downstream while still being upstream of the parts of the chain where delay bias arises. By use of software developed for the purpose, the receiver continuously determines the delay bias by tracking the L1 and L2 versions of the GLONASS signal.

This work was done by Courtney B. Duncan, Thomas K. Meehan, and Donovan J. Spitzmesser of Caltech for NASA's Jet Propulsion Laboratory. Further information is contained in a TSP [see page 1].

In accordance with Public Law 96-517, the contractor has elected to retain title to this invention. Inquiries concerning rights for its commercial use should be addressed to

Technology Reporting Office
JPL
Mail Stop 122-116
4800 Oak Grove Drive
Pasadena, CA 91109
(818) 354-2240

Refer to NPO-20058, volume and number of this NASA Tech Briefs *issue, and the page number.*

BLANK PAGE

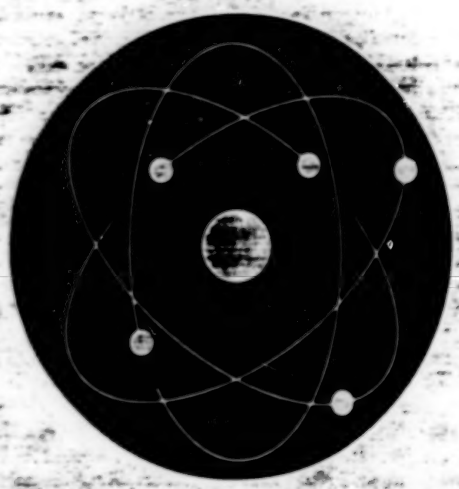

Physical Sciences

Hardware, Techniques, and Processes

Books and Reports

BLANK PAGE

Advanced Electromagnetic Probes for Characterizing Materials

Properties of materials and thicknesses of subsurface layers can be measured nondestructively.

Goddard Space Flight Center, Greenbelt, Maryland

Two types of advanced electromagnetic sensors that operate in quasistatic spatial modes have been developed for use in nondestructive characterization of materials in surface and subsurface layers and for determining the thicknesses of the layers. Because the sensors are thin and flexible, they conform readily to curved surfaces, making it possible to inspect complexly shaped specimens (see Figure 1) that could include regions that would otherwise be accessible only with difficulty. The sensor outputs can be analyzed according to continuum mathematical models of the interactions between the sensor electromagnetic fields and the layered media to obtain repeatable quantitative measures of such physical and geometric properties as electrical conductivity, permeability, porosity, roughness, coating thickness, residual stress, and surface flaws.

The sensors of one type, called "meandering-winding magnetometers" (MWMs), can be used as either (1) eddy-current sensors to measure electrical properties of conductive materials or (2) magnetic sensors to measure magnetic properties of conductive or nonconductive materials. Each MWM includes a primary (driver) winding that meanders (in a plane, except, of course, when the sensor is bent to conform to a surface). Secondary (sensing) windings meander along the primary winding on both sides (see Figure 2). The primary winding is driven by a known input current at a prescribed frequency. The voltage at the terminals of the secondary windings is measured and used to determine the magnitude and phase of an impedance that is defined as the ratio between the secondary voltage and the primary current. The magnitude and phase of this impedance yield information about the magnetic and conductive media penetrated by the applied magnetic field.

The sensors of the other type, called "inter-digital electrode dielectrometers" (IDEDs) enable the use of electric fields to measure the permittivities and the small residual conductivities of materials that are regarded as electrical insulators. Each IDED includes two electrodes laid out as interdigitated fingers on a polyimide substrate. While one electrode (the driving electrode) is excited with a known sinusoidal voltage at a prescribed frequency, the voltage on the other electrode (the sensing electrode) is measured. The phase shift and the ratio between the amplitudes of voltages on the two electrodes provide information about the dielectric materials penetrated by the applied electric field.

Figure 1. A Probe Containing an MWM can be used to inspect a specimen with a concave, convex, conical, or flat surface.

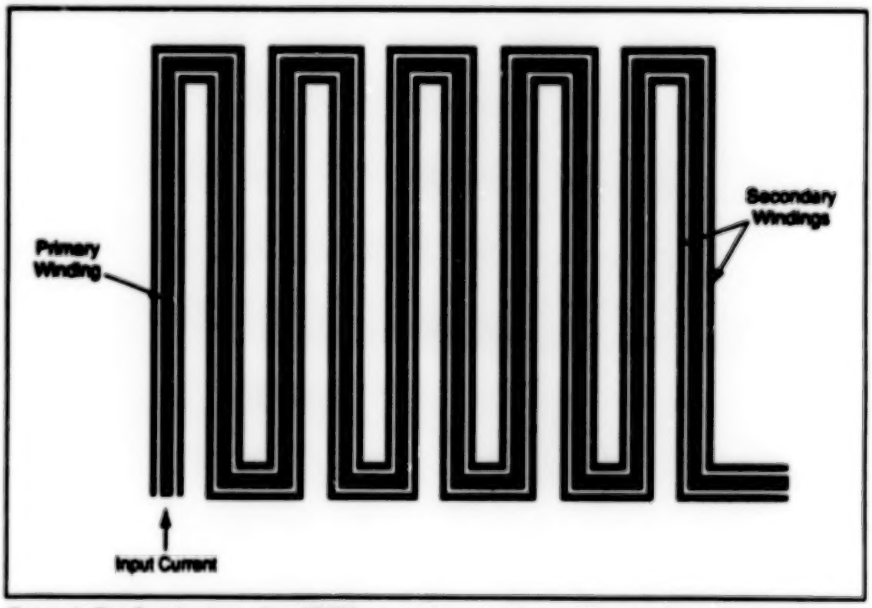

Figure 2. The Conductors of an MWM act as primary and secondary windings of a transformer, the magnetic field of which penetrates the specimen on which it is placed.

The depth of penetration of the electric field of an IDED depends only on the elec-

trode spacing. Multiple IDEDs with different electrode spacings for different depths of penetration can be used to characterize dielectric properties and changes in those properties as functions of depth, even for such heterogeneous materials as composites.

Given (1) the geometries of MWM windings and IDED electrodes, (2) the driving frequencies, (3) the properties and dimensions of specimens, and (4) the MWM and IDED mathematical models, one can generate lookup tables, called "measurement grids," for calibration of sensor outputs. Measurement grids can be used to convert sensor outputs directly into estimates of layer thicknesses and electromagnetic properties. Layer thicknesses can include, for example, thicknesses of surface coatings, thicknesses of air gaps between metallic layers, and lift-off distances between sensors and specimen surfaces.

Applications of MWMs and IDEDs include the following:

- Characterization of coatings on metals, ceramics, and composites;
- Monitoring for fatigue, corrosion, and thermal damage indicative of deterioration with age;
- Process monitoring to detect plastic deformation (e.g., as a result of shot peening), porosity, and heat-affected zones;
- Noncontact measurement of temperature in regions to which access would otherwise be difficult;
- Detection and measurement of sizes of cracks; and
- Measurement of anisotropy of selected properties of heterogeneous materials under bidirectional loads.

Thickness measurements have been demonstrated on a variety of intermetallic and ceramic coatings, including a nickel/aluminum alloy on aluminum substrates and zirconia/yttria on 304 stainless-steel substrates. Potential uses of MWMs and DEDs include inspection of turbine blades, reactor tubes, airframe structural components, and other critical components in the aerospace and power-generation industries.

This work was done by Neil J. Goldfine of JENTEK Sensors, Inc., for Goddard Space Flight Center. Further information is contained in a TSP [see page 1].
GSC-13878

Portable Instrument Measures Ice Profiles

Accurate measurements can be performed rapidly, with minimal labor.

Lewis Research Center, Cleveland, Ohio

A portable optoelectronic instrument measures profiles of ice deposits that have formed on leading edges of airfoils in the Icing Research Tunnel at Lewis Research Center. Previously, technicians working in the cold, wet environment of the tunnel measured these profiles in a tedious manual procedure: An aluminum block was used to melt a section of ice so that a card could be placed against the ice, then a pencil was used to trace the profile of the ice onto the card. The melting affected the profile, and the tracing process was time-consuming and subject to human error.

The instrument satisfies a need to measure the ice profiles accurately and rapidly, and to be readily operable by technicians, with minimal labor. The instrument (see figure) includes four low-power, eye-safe laser diodes that project a thin red (wavelength 670 nm) line onto the ice to be measured. Three computer-controlled charge-injection-device video cameras and a frame grabber capture the image of the ice shape (as illuminated by the diode lasers) from three different positions.

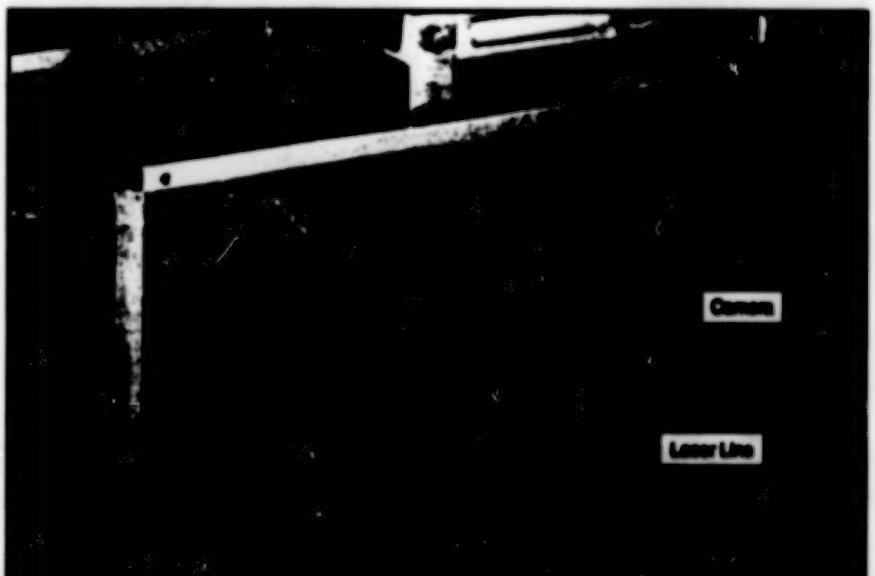

An Illuminated Line on the surface to be measured is imaged in three video cameras. The image data are processed to quantify the profile of the surface.

A microcomputer (Compaq 80386, or equivalent) running custom software merges the images from the three cameras and corrects for distortions associated with the camera angles. The profile is displayed on the computer screen and saved in an ASCII file on hard disk. The technician has the option of printing a 1:1-scale profile of the ice shape. The profile is accurate to within 1 percent. The entire profiling process takes about one minute.

This work was done by Mario Vargas of Lewis Research Center and Edward A. Hovenac of NYMA, Inc. No further documentation is available.

Inquiries concerning rights for the commercial use of this invention should be addressed to the Patent Counsel, Lewis Research Center [see page 1]. Refer to LEW-16117.

Holographic Acoustic Microscopy for Microelectronics

Acoustic diffraction and interference would be exploited to image features inside complex microelectronics.

NASA's Jet Propulsion Laboratory, Pasadena, California

Holographic acoustic microscopy (HAM) has been proposed as a method for inspection and analysis of dense microelectronic circuits. Whereas previous developments in acoustic microscopy have yielded a capability for generating two-dimensional images the proposed development would result in the generation of three-dimensional images, in which one could see features that previously would have been hidden by other features that cast acoustic shadows. For example, HAM could yield detailed images of cracks.

HAM would involve adaptation of concepts and techniques from both three-dimensional optical holography and scanning laser acoustic microscopy (SLAM). The imaging wavefronts would be generated according to the principles of optical holography, except that phonons would be used instead of photons, and the wavefront information would be recorded by use of modified SLAM transducers and a modified SLAM imaging system instead of a photographic plate.

The figure illustrates one of several alternative HAM setups. The microelectronic device or other object to be examined would be suspended in a liquid couplant — typically, water. Two acoustic transducers would be excited at the same frequency and in coherent in phase. One acoustic transducer would launch a reference acoustic signal, analogous to a reference beam in optical holography; this signal would not go through the object, but would pass unhindered to the surface of the water, where it would give rise to ripples. The other transducer would launch an acoustic signal that would pass through and be diffracted by the object on its way to the surface, giving rise to a second ripple pattern superimposed on the first one. The net ripple pattern would constitute the hologram.

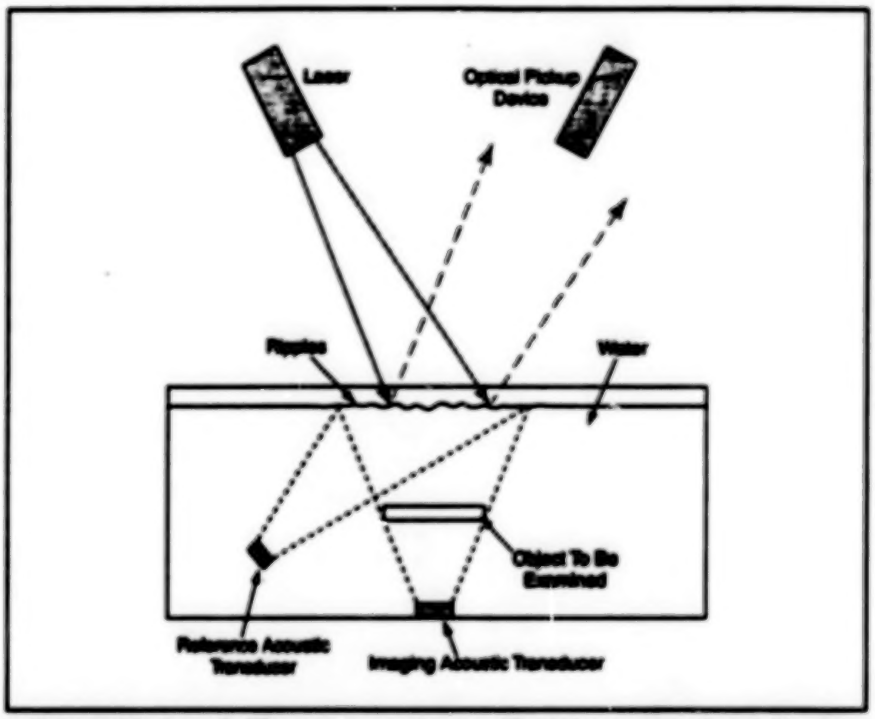

In Holographic Acoustic Microscopy, sound waves diffracted on passage through the object would interfere with sound waves that did not pass through the object, producing a hologram in the form of a ripple pattern on the surface of the water.

A laser beam amplitude-modulated at the acoustic frequency would be rastered across the hologram and the light diffracted by the hologram would be detected by an optical pickup device. If the laser light were amplitude-modulated and optically manipulated such that the complex amplitude of its modulation at each point along the raster were proportional to the complex conjugate of the complex amplitude of the reference acoustic signal at that point, then the amplitude of the light diffracted by the hologram at that point would be proportional to the acoustic signal diffracted by the object and reaching that point. Alternatively, optical reconstruction could be effected in real time by use of reflection of coherent light from the surface of the water.

This work was done by John D. Olives of Caltech for NASA's Jet Propulsion Laboratory. Further information is contained in a TSP [see page 1].

NPO-20118

Miniature Directional Hydrophones

Micromachined tunneling transducers are housed between titanium hemispheres.

NASA's Jet Propulsion Laboratory, Pasadena, California

Miniature low-noise, neutrally buoyant, directional hydrophones are undergoing development. A prototype miniature hydrophone is contained in a spherical titanium shell (see figure) with a volume of about 0.52 in.^{3} (8.6 cm^3). These miniature hydrophones are intended to replace older hydrophones contained in packages with volumes of about 20 in.^{3} (328 cm^3).

The sensors in the miniature hydrophones are micromachined tunneling accelerometers like those described in "Dual-Element Tunneling Accelerometer" (NPO-18662), *NASA Tech Briefs*, Vol. 18, No. 11 (November 1994), page 36 and "Dual-Element Tunneling Accelerometer With Dual Feedback (NPO-19259) *NASA Tech Briefs*, Vol. 21, No. 2 (February 1997), page 55. The compactness, sensitivity, and low self-noise of the tunneling accelerometers makes it possible to achieve the desired miniaturization while retaining the desired level of performance.

In assembling the prototype miniature hydrophone, the accelerometers plus feedback control and other electronic circuits are mounted on a in a lightweight

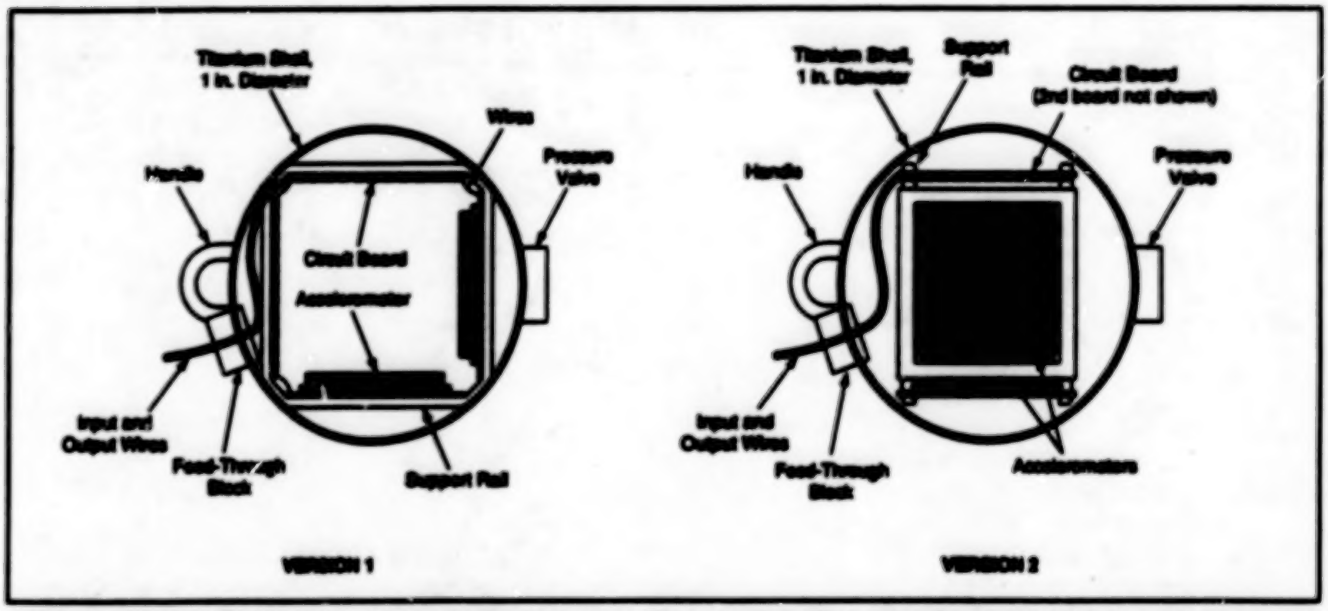

A Spherical Titanium Shell contains a miniature directional hydrophone. The two versions differ in the configurations in which the accelerometers and circuit boards are bonded to the support rails. In this example, the two accelerometers provide sensitivity to accelerations along two orthogonal axes.

frame, and the resulting assembly is bonded inside one of two hemispherical titanium shells. Input and output wires pass through a feed-through block on the shell and are connected to the circuits inside the shell. The two hemispherical shells are then bonded together to make a single spherical shell that can be evacuated and can withstand external pressure of 1,000 psi (6.9 MPa).

This work was done by Thomas W. Kenny, William J. Kaiser, Howard W. Rockstad, Joseph K. Reynolds, Elaine Lindstal, and Timothy E. Cushing of Caltech for NASA's Jet Propulsion Laboratory. Further information is contained in a TSP [see page 1].

NPO-19678

Compact Off-Axis Relay for Adaptive Optics

This design provides an accessible pupil location and simplifies alignment.

NASA's Jet Propulsion Laboratory, Pasadena, California

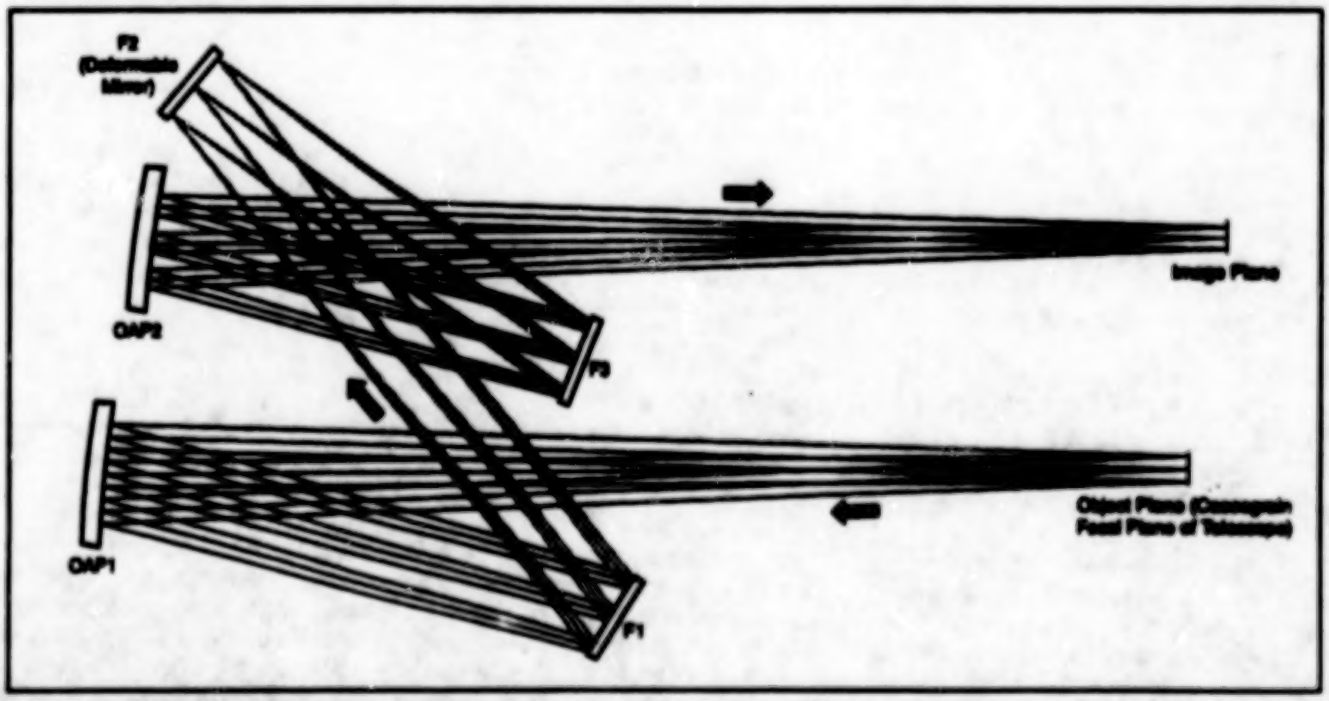

This Ray-Trace Diagram shows the layout of the relay, which features compactness, accessibility of pupil location, ease of alignment, and minimization of the number of reflections.

An optical relay has been designed to provide coupling between a deformable mirror and a Cassegrain astronomical telescope. The deformable mirror is part of a system of adaptive optics for real-time correction of optical wavefront distortions caused by turbulent variations in the index of refraction of the atmosphere. The relay is an unobscured optical subsystem with a magnification of –1. It provides a pupil plane conjugate to the primary mirror of the telescope, with proximate object and image planes. The pupil plane is intended to be the location of the deformable mirror.

The relay (see figure) includes a pair of off-axis paraboloidal mirrors and three flat mirrors in an unusually compact, folded arrangement. Rays coming from the Cassegrain focus of the telescope are recollimated by the first off-axis paraboloidal mirror (OAP1). The recollimated rays are folded by three flat mirrors (F1, F2, and F3) and are then reimaged at the original focal ratio by the second off-axis paraboloidal mirror (OAP2). In addition to recollimating the Cassegrain-focused rays, OAP1 also forms a pupil conjugate to the telescope primary mirror at F2, where the deformable mirror is placed.

Because of a limitation on actuator strokes in the deformable mirror, an independent tip/tilt mirror is usually needed. The location of F1 is an ideal location for the placement of this tip/tilt mirror. The location of F3 is also available for a second deformable mirror in a multiconjugate adaptive optical system, which can correct for atmospheric turbulence at different altitudes and thereby increase the angular size of the corrected field.

An auxiliary benefit of this design is that through appropriate selection of the angles of the flat mirrors, the axes of symmetry of the two off-axis paraboloids can be made parallel to each other. This parallelism eases alignment in that it makes it possible to align the two off-axis paraboloids by use of a single jig that carries a retroreflecting mirror or other appropriate alignment apparatus, with a simple linear translation of the jig between the two axes. In another, related technique, a sufficiently wide alignment beam could be used to illuminate both off-axis paraboloids simultaneously, and the return signals would be used to align their respective axes.

This work was done by Richard G. Delaney of Caltech for NASA's Jet Propulsion Laboratory. Further information is contained in a TSP [see page 1].

NPO-19943

Improved Model for Hot-Electron-Bolometer Mixer

Electrons and phonons are characterized by two different temperatures.

NASA's Jet Propulsion Laboratory, Pasadena, California

An improved theoretical model has been developed to represent the photoresponse of a quasi-optical signal-mixing device of the hot-electron-bolometer type. More specifically, the model pertains to a device in which two input signals with frequencies of the order of 2.5 THz that differ by an amount of the order of 2.5 GHz impinge a submicron-sized bridge (microbridge) made of a film of the high-critical-temperature (high-T_c) superconductive material $YBa_2Cu_3O_{7-\delta}$ about 10 nm thick between normally conductive metal contacts on a highly thermally conductive substrate on a heat sink. The impinging signals cause nonequilibrium heating of the electron gas in the microbridge. Due to strong local oscillator pumping, the electron temperature is close to T_c; therefore, this nonequilibrium heating causes variations in the electrical resistance of the microbridge, resulting in mixing of the signals to generate a signal at the difference frequency of about 2.5 GHz.

The model accounts for heating of both the electrons and the crystalline lattice of the $YBa_2Cu_3O_{7-\delta}$ film, and for diffusion of heat through the film to both the substrate and the normally conductive metal contacts (see figure). The electron and phonon populations are characterized by temperatures T_e and T_p, respectively; in the nonequilibrium environment, these temperatures can differ from each other and from the temperature of the substrate.

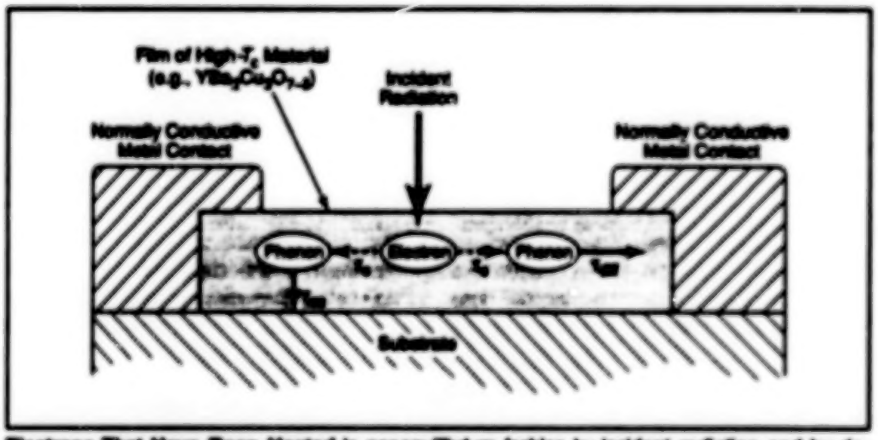

Electrons That Have Been Heated in nonequilibrium fashion by incident radiation and by dc transport are cooled by interaction with phonons, some of which escape to the substrate, others of which diffuse to the normally conductive metal contacts.

The figure illustrates the principal heat-removal processes taken into account in the model. Unlike in Nb superconductive microbridges that operate at much lower T_cs (of the order of 5 K), electron diffusion contributes little to the removal of heat in the high-T_c case. Measurements have shown that the resistive response can be described in terms of (1) relaxation of the T_e via interaction with phonons with a characteristic time, τ_e of about 1 to 2 ps at typical T_c between 80 and 90 K and (2) a slower relaxation of T_p by escape of phonons to the substrate with a characteristic time that depends on the dimensions of the $YBa_2Cu_3O_{7-\delta}$ film and the substrate material. Some nonequilibrium phonons escape from the $YBa_2Cu_3O_{7-\delta}$ film through the film/substrate boundary with a characteristic time τ_{es}, while others diffuse to the normal-metal contacts with a characteristic time τ_{en}. Yet another thermal process that affects the relaxation time and the total thermal resistance of the microbridge is the diffusion of heat (via phonons) in the substrate.

The model incorporates coupled nonlinear differential equations for T_e and T_p as functions of time. These equations can be solved to evaluate the performances of microbridges with various design parameters under various operating conditions. In particular, the model has been used to study all important mixer parameters for a

practical range of operating conditions needed for a 2.512-THz heterodyne receiver that would be used to measure the concentration of OH radicals in the upper atmosphere. It has been shown that a microbridge mixing device like the one described above could be made to exhibit a very low noise temperature (~2,000 K) and to consume only microwatts of local-oscillator power.

This work was done by Boris S. Karasik, William R. McGrath, and Michael C. Gaidis of Caltech for NASA's Jet Propulsion Laboratory. Further information is contained in a TSP [see page 1].
NPO-20045

Laser-Based Techniques for Research on Combustion

Concentrations of soot and polycyclic aromatic hydrocarbons can be spatially and temporally resolved.

Lewis Research Center, Cleveland, Ohio

LII Excited by 1,064-nm Laser, Viewed at 400 nm

LIF and LII Excited by 355-nm Laser, Viewed at 400 nm

LIF and LII Excited by 355-nm Laser, Viewed at 600 nm

An Ethylene/Air Diffusion Flame just above the end of a tube was imaged by LIF and LII at various wavelengths. The small intervals of the ruler are millimeters.

Laser-induced incandescence (LII) and laser-induced fluorescence (LIF) have been found to constitute a valuable combination of techniques for research on combustion processes. These techniques can be used to obtain temporally resolved images of concentrations of polycyclic aromatic hydrocarbons (PAHs) and of soot in flames and exhaust gases. Spatially resolved quantitative data on the concentrations can be extracted from the images. These data are important because concentrations of PAHs and soot are indicative of basic physical and chemical combustion mechanisms and of the performances of combustors. For example, soot necessarily forms from PAH precursors, and both soot and PAHs are major constituents of combustion-related atmospheric pollution.

LIF yields information on PAH concentrations, while LII yields information on soot concentrations. [The use of LII to measure the spatially and temporally resolved concentration of soot in a flame was reported previously in "Laser-Induced Incandescence for Research on Combustion" (LEW-16078), *NASA Tech Briefs*, Vol. 20, No. 12 (December 1996), page 16a.] Depending upon the specific experiment that one wants to perform, one can use either LII or LIF separately, or one can use both techniques simultaneously to obtain more information than can be obtained by either technique alone, as explained below.

If a single pulse of ultraviolet laser light is used for excitation, then both LIF and LII signals can be detected during and shortly after the pulse. The LII signal decays more slowly than the LIF signal does; this feature can be used to distinguish between the LIF and LII responses. If a single pulse of near-infrared laser light is used for excitation, then only a LII response is observed during and shortly after the pulse. When infrared and ultraviolet pulses are used in measurements, then the difference between the combined ultraviolet-excited LIF/LII image and the infrared-excited LII (only) image can yield an LIF image.

LIF and LII can be observed and measured by use of images acquired by intensified cameras, relying on the excitatory laser pulses to provide temporal resolution. The use of LII and LIF in various excitation/detection schemes was demonstrated in experiments on a well-understood gas-jet diffusion flame, in which ethylene flowed out of a brass tube and burned in a surrounding co-flow of air. In each experiment, the laser beam was formed into a sheet to illuminate a cross section of the flame just above the end of the tube. A gated, intensified camera was used to view the LIF and/or LII coming from the illuminated cross-sectional plane. The figure contains three images acquired under different excitation/detection conditions, as follows:

The first image shows LII (only) excited by a laser beam at a wavelength of 1,064 nm and viewed through a band-pass interference filter centered at a wavelength of 400 nm. This image reveals soot in a thin annular region typical of diffusion flames.

The second image shows simultaneous LIF and LII excited by a 266-nm laser, also viewed through the 400-nm band-pass filter. This image reveals both the annular distribution of soot and the distribution of PAHs in the fuel-rich region surrounded by the annular soot shell.

The third image shows simultaneous LIF and LII excited by a 266-nm laser and viewed through another band-pass interference filter at a wavelength of 600 nm. The LII (soot) component of this image resembles that of the preceding image, but the LIF (PAH) component appears concentrated closer to the region containing the soot; this result is consistent with (a) the previous observation that larger PAH molecules tend to fluoresce at greater wavelengths, coupled with (b) the hypotheses that the basic physical and chemical mechanisms of the flame should result in concentration of larger PAH molecules toward the outer region where soot forms.

This work was done by Randy L. Vander Wal of NYMA, Inc., for Lewis Research Center. Further information is contained in a TSP [see page 1].

Inquiries concerning rights for the commercial use of this invention should be addressed to NASA Lewis Research Center, Commercial Technology Office, Attn: Tech Brief Patent Status, Mail Stop 7-3, 21000 Brookpark Road, Cleveland, Ohio 44135. Refer to LEW-16302.

Acousto-Ultrasonic Monitoring of Ceramic Composites

The progression of damage under dynamic loads can be monitored during tests.

Lewis Research Center, Cleveland, Ohio

The acousto-ultrasonic (AU) technique has been found to be useful for assessing the state of damage and for real-time monitoring of the progression of damage in specimens of ceramic composite materials subjected to dynamic loads. The real-time AU technique could be used, for example, in fatigue tests to study the growth of subcritical flaws and other failure mechanisms in ceramic composites. Though the tests may be destructive, the AU technique is nondestructive.

Developed previously for non-real-time applications, the AU technique is a hybrid of acoustic-emission and ultrasonic techniques. The figure schematically illustrates a typical AU laboratory setup and the associated flow of information. Repeated ultrasonic pulses are excited at one location along a specimen by use of a broad-band transmitting transducer. The stress waves associated with these pulses propagate along the specimen to a receiving transducer; along the way, the stress waves interact with the microstructure and flaws present between the transducers. The received signal can be analyzed to evaluate the damage and flaws.

The analysis is formulated to yield parameters called "stress wave factors" (SWFs), which can be related quantitatively to the mechanical performance of the specimen material. An SWF is a measure of stress-wave energy transmission and of the efficiency with which dynamic strain energy is transferred in the material. In a comparison with a material that exhibits given SWF values, a material that exhibits greater SWF values is more capable of transmitting dynamic stress or redistributing loads and thus can be expected to be stronger. Conversely, lower SWF values indicate regions where dynamic strain energy is likely to become concentrated and promote fracture.

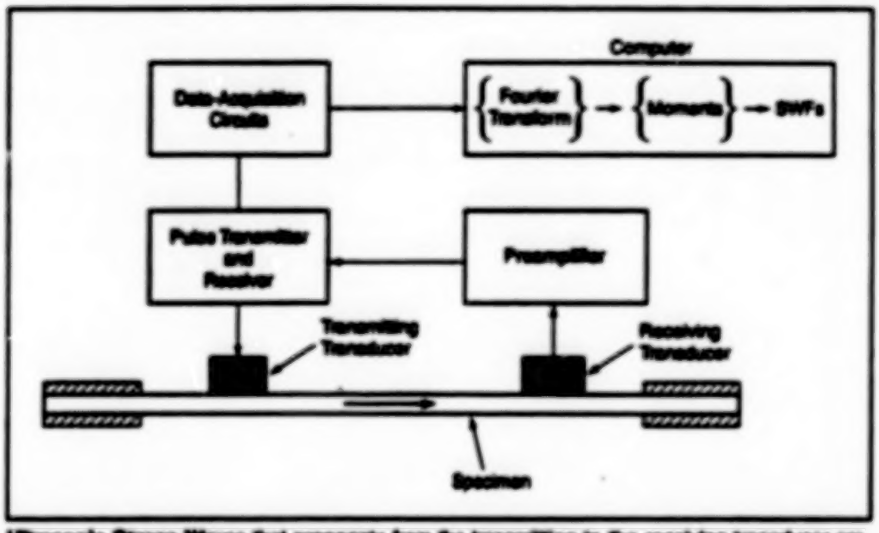

Ultrasonic Stress Waves that propagate from the transmitting to the receiving transducer are altered by the intervening specimen material. The output of the receiving transducer is analyzed to extract information on damage and flaws along the propagation path.

In the present AU technique, the output voltage of the receiving transducer as a function of time is digitized and converted to an amplitude-vs.-frequency spectrum via a Hartley transform. Various statistical moments of the frequency spectrum are then computed; these moments constitute the SWF values.

Prior to the development of the real-time AU technique, it was common practice to interrupt a mechanical test, then perform AU and other nondestructive tests before resuming the test at the next load level. In the real-time AU technique, one continues to excite pulses and process the output of the receiving transducer throughout a mechanical test, which is performed without interruption. The progression of damage is monitored by observing the changes in the SWFs computed from the received AU signals.

A mathematical model of acousto-ultrasonic stress-strain response (AUSSR) in unidirectional and cross-ply composite materials has been formulated. The model utilizes real-time AU data and classical laminated-plate theory to predict strain responses to increasing stress levels. Weibull parameters in the AUSSR model can be used to calculate design stresses for thermostructural applications. Real-time AU and the AUSSR model can be used to study failure mechanisms in specimens under quasi-static and fatigue loads.

This work was done by George Baaklini of Lewis Research Center and Anil Tiwari and Edmund G. Henneke of Virginia Polytechnic Institute and State University. Further information is contained in a TSP [see page 1].

Inquiries concerning rights for the commercial use of this invention should be addressed to NASA Lewis Research Center, Commercial Technology Office, Attn: Tech Brief Patent Status, Mail Stop 7-3, 21000 Brookpark Road, Cleveland, Ohio 44135. Refer to LEW-16451.

Two-Wavelength Pyrometry With Self-Calibration

Knowledge of instrument gain, emissivity, and transmissivity are not necessary for determining temperature.

Lewis Research Center, Cleveland, Ohio

An improved method of two-wavelength optical pyrometry provides for the determination of different temperatures of a specimen surface at different times. Unlike in other pyrometric methods, there is no need for explicit knowledge of such ancillary wavelength-dependent parameters as emissivity of the specimen surface (or ratios between emissivities at different wavelengths) and transmissivity of the optical path from the specimen to the pyrometer. There is also no need for explicit knowledge of the wavelength-dependent voltage response of the pyrometer; in other words, it is not necessary to calibrate the pyrometer. Instead, the method provides for self-calibration through the generation and use of implicit calibration information

from pyrometer readings at two wavelengths and at two or more different temperatures.

The method requires a pyrometer in the form of a spectrometer, plus a computer to acquire and process the pyrometer readings. The method is based on (a) Planck's radiation law as modified for wavelength-dependent emissivity and transmissivity, and (b) the fundamental equation for the response of the pyrometer. Planck's radiation law can be expressed as

$$L(\lambda,T)=\frac{\varepsilon_\lambda\tau_\lambda c_1}{\lambda^5\left[\exp\left(\frac{c_2}{\lambda T}\right)-1\right]}$$

where $L(\lambda,T)$ is the spectral intensity of the radiation at wavelength λ arriving at the pyrometer, T is the absolute temperature of the emitting surface of the specimen, ε_λ is the wavelength-dependent emissivity of the specimen surface, τ_λ is the wavelength-dependent transmissivity of the optical path, and c_1 and c_2 are fundamental physical constants. The voltage response of the pyrometer to the incident radiation at wavelength λ is given by

$$V(\lambda)=g_\lambda L(\lambda,T)$$

Let the unknown wavelength-dependent parameters g_λ, ε_λ, and τ_λ be lumped into one wavelength-dependent term via

$$A(\lambda)=g_\lambda\varepsilon_\lambda\tau_\lambda$$

Let pyrometer readings be taken at wavelengths λ_1 and λ_2 at two different times (0, $t_1, t_2, \ldots, t$) when the temperatures of the specimen [$T(0), T(t_1), T(t_2), \ldots, T(t)$] are different. By combining and manipulating the foregoing equations, one can show that the four pyrometer readings are related by the following equation:

$$\frac{V(\lambda_1,0)}{V(\lambda_1,t)}=\frac{\left[1+\frac{A(\lambda_2)}{V(\lambda_2,t)}\right]^{\frac{\lambda_2}{\lambda_1}}+1}{\left[1+\frac{A(\lambda_2)}{V(\lambda_2,0)}\right]^{\frac{\lambda_2}{\lambda_1}}+1}$$

Least-squares curve fitting of the quantity

$$y(t)=\frac{V(\lambda_1,0)}{V(\lambda_1,t)}=\frac{\left[1+A(\lambda_2)x(t)\right]^{\frac{\lambda_2}{\lambda_1}}+1}{\left[1+\frac{A(\lambda_2)}{V(\lambda_2,0)}\right]^{\frac{\lambda_2}{\lambda_1}}+1}$$

versus the quantity

$$x(t)=\frac{1}{V(\lambda_2,t)}$$

from $t = 0$ to time $= t$ determines the quantity $A(\lambda_2)$. One can also formulate this equation with the roles of λ_1 and λ_2 interchanged and solve the equation to obtain $A(\lambda_1)$. Thereafter, one can compute the instantaneous temperature directly from a pyrometer reading at either wavelength, using

$$T=\frac{c_2}{\lambda\ln\left[1+\frac{A(\lambda)}{V(\lambda)}\right]}$$

This work was done by Daniel Ng of Lewis Research Center. Further information is contained in a TSP [see page 1].

Inquiries concerning rights for the commercial use of this invention should be addressed to the Patent Counsel, Lewis Research Center [see page 1]. Refer to LEW-16182.

Books and Reports

Secondary Electron Emission From Thin Diamondlike Films

A report describes experiments on secondary electron emission (SEE) from specimens comprising various thin diamond and diamondlike carbon films on molybdenum and silicon substrates. Each specimen was mounted in a vacuum, biased at a potential of –50 V, and bombarded with a primary beam of electrons. The secondary-electron coefficient (σ) was determined as a function of time for various values of the beam currents at primary-beam electron kinetic energies from 100 to 3,000 eV. As-deposited specimens of diamond on Mo exhibited $\sigma = 14$. The value of σ was about 2 for a specimen of boron-doped, plasma-etched diamond on Si, but about 6 for a specimen of (100) diamond on Si; this suggests that secondary electron emission depends on microstructure. Heating in a vacuum increased σ in previously undamaged diamond/Mo specimens to 27. Secondary yields were found to decrease with exposure to the electron beam, at a rate proportional to the beam current. Subsequent prolonged exposure to H_2 was found to restore σ to initial or higher values. Consistently with the notion that secondary electrons are emitted from within an escape depth of the surface, σ was found to vary with the angle of incidence of the electron beam. Since its completion, a lot of new research has been accomplished on SEE of diamond and diamond films. Any new related information can also be obtained via sources listed below.

This work was done by Isay L. Krainsky and James Dayton of Lewis Research Center and Gerald Mearini of Case Western Reserve University. To obtain a copy of the report, "Study of Electrical Phenomena Associated With Thin Films," see TSP's [page 1].

Inquiries concerning rights for the commercial use of this invention should be addressed to NASA Lewis Research Center, Commercial Technology Office, Attn: Tech Brief Patent Status, Mail Stop 7–3, 21000 Brookpark Road, Cleveland, Ohio 44135. Refer to LEW-16514.

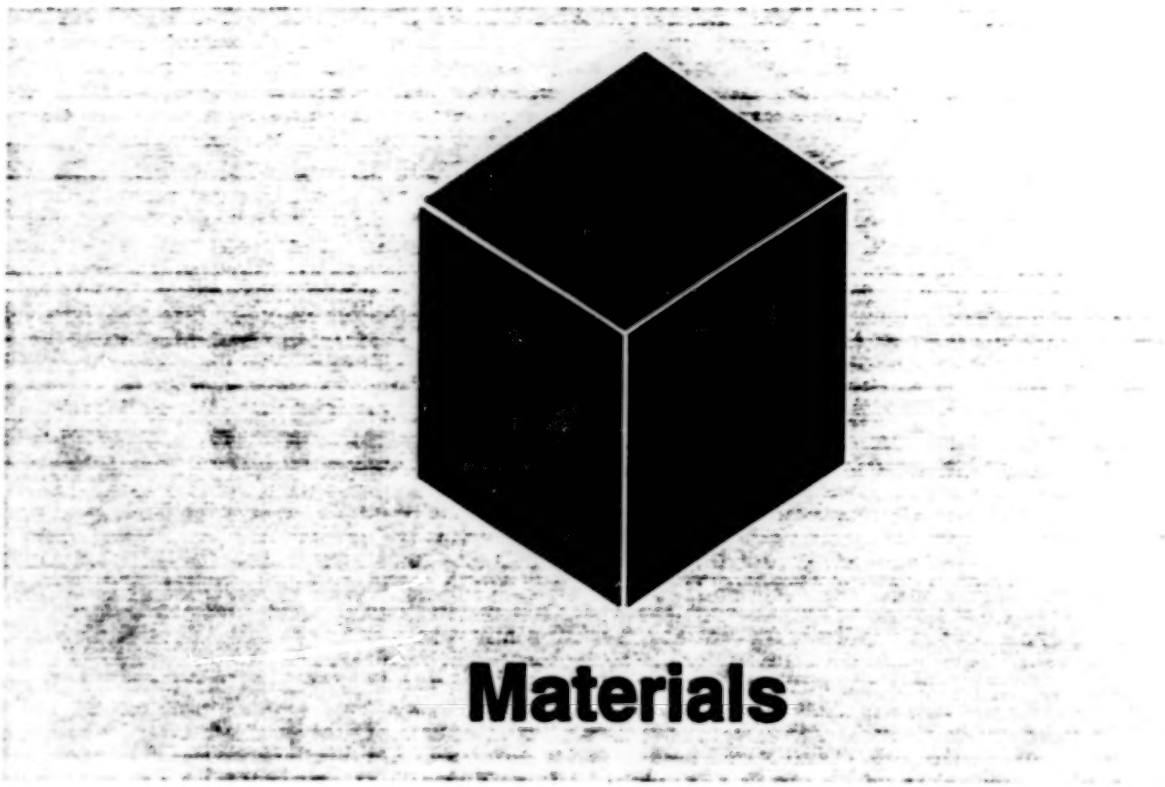

Materials

Hardware, Techniques, and Processes

Books and Reports

BLANK PAGE

Simplified Micromechanics of Plain-Weave Composites

Mechanical, thermal, and hygral behavior can be estimated with less computation.

Lewis Research Center, Cleveland, Ohio

A micromechanics-based method has been developed to facilitate numerical simulation of the mechanical, thermal, and hygral responses of plain-weave matrix/fiber laminated composite materials. The equations obtained via this method are meant to be used in combination with micromechanics-based computer codes like Integrated Composite Analyzer (ICAN), which has been described previously in *NASA Tech Briefs*. Because it is based on micromechanics, this method affords the capability for mathematically modeling stresses and strains at any level of detail from a microscopic scale within an individual fiber or interfiber matrix to a macroscopic laminate. The main advantage of this method is that micromechanics is based on closed-form equations and thus offers high computational efficiency, relative to a detailed three-dimensional finite-element formulation.

As used here, "plain-weave" pertains to a fabric in which a warp or longitudinal fiber tow is interlaced with every second fill or transverse fiber tow. A representative volume element or unit cell (see figure) based on the repeating unit of the plain-weave-fabric component of a composite is used to construct a mathematical model of the micromechanics in this method. The model accounts for the undulations of the fiber tows and the distributions of fiber ends through the thickness. In applying the basic equations of micromechanics, it is assumed that the classical laminate plate theory is applicable in thin sections defined by slices orthogonal to the *x* axis. Each section is further sliced in its *x*-*z* plane, the properties of each slice are computed as though each were a ply in a laminate, then the properties of the stacked of slices are computed to obtain the properties of each section.

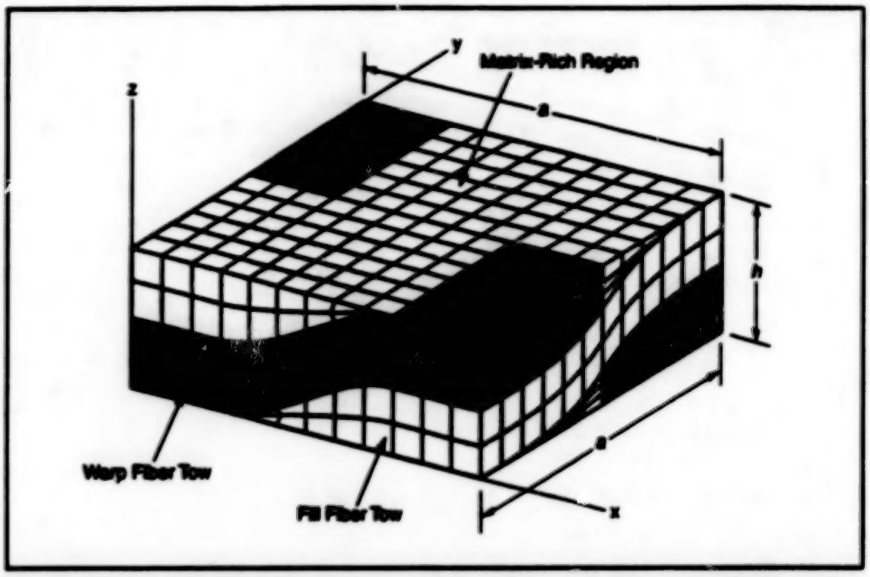

One-Fourth of a Unit Cell derived from the periodic structure of a plain-weave fabric is used in the micromechanics-based analysis. The rest of the unit cell is modeled by copying the results from this portion, invoking arguments of symmetry.

For a stress analysis, a laminate analysis is performed with an applied load to obtain equivalent slice stresses in warp and fill regions. Optionally, one can then perform a micromechanics-based analysis again to divide the stresses in the warp and fill regions into fiber and matrix microstresses. Thus, one can simulate responses at any level of detail. All the features that are already incorporated into ICAN or another composite-analysis code for modeling such phenomena as effects of processing, voids, environmental degradation, and effects of cyclic loads can be incorporated easily into an analysis by the present method. In a comparison involving a graphite/epoxy and a SiC/SiC plain-weave composite, the present method was found to yield predictions similar to those of detailed three-dimensional finite-element analyses and in reasonably close agreement with limited experimental data.

This work was done by Pappu L. N. Murthy and Christos C. Chamis of Lewis Research Center and Subodh K. Mital of the University of Toledo. Further information is contained in a TSP [see page 1].

Inquiries concerning rights for the commercial use of this invention should be addressed to NASA Lewis Research Center, Commercial Technology Office, Attn: Tech Brief Patent Status, Mail Stop 7–3, 21000 Brookpark Road, Cleveland, Ohio 44135. Refer to LEW-16435.

Guanidine: a Unique Strong Organic Base

Guanidine can be used in place of NaOH and KOH in some applications.

Lewis Research Center, Cleveland, Ohio

Guanidine [$NH_2C(:NH)NH_2$] is an organic base with a strength equal to that of sodium hydroxide. Guanidine can be used as a substitute for alkali metal hydroxides in making ceramics in which residual sodium or potassium ash would be detrimental, because guanidine and its organic derivatives can be removed thermally, without leaving residues. Ceramics in which sodium or potassium ash would be detrimental include those in which resistance to oxidation must be combined with high strength, and ceramic superconductors, which must be pure to have high critical-current capacities. Guanidine can also be used in the recovery of cations (using the guanidine form of cation-exchange resins), as an additive for electroplating, and as a soap for lubricants.

Ceramic articles are generally fabricated from powders by a variety of processes that include slip casting, injection molding, and doctor blading. In most cases, ionic organic chemicals are used in these

processes as deflocculants and binders to form "green" (unfired) bodies of adequate strength to permit handling prior to firing. Many organic processing aids contain alkali metal cations — usually sodium, which remains in ash in the fired products. These impurities degrade the high-temperature performances of the finished articles — a shortcoming that can be prevented by use of guanidine and guanidine derivatives instead of metal hydroxides.

The following three classes of guanidine derivatives have been found to be useful in making ceramics:

- Guanidine oxalate: useful as a reagent for making intimate oxide mixtures. The metal oxalates, which serve in this case as precursors to metal oxides, are coprecipitated in one step and then thermally decomposed into oxides. This technique can be used to make easily sinterable oxide powder mixtures. Guanidine oxalate coprecipitation has been used to produce high-grade $YBa_2Cu_3O_{7-x}$ superconducting powder, intimate Sr/La/Cu powder mixtures, and yttria-doped cerium(III) oxide.
- Guanidine polyelectrolytes (guanidine polyacrylate) and surfactants: These are excellent deflocculants and binders for making ceramics. Guanidine polyacrylate is a good deflocculant and binder for uncontaminated ceramic slurries used for slip casting, injection molding, and doctor blading. Such ionic polyelectrolytes as guanidine polyacrylate have been found to provide excellent "green"-body strength.
- Guanidine soaps, which are guanidine salts of organic fatty acids: These can be used as vehicles and binders for coating substrates with oxides and noble metals. The guanidine fatty acid salt guanidine 2-ethyl-hexanoate has been found to be a useful vehicle and binder for coating alumina (sapphire) fibers with zirconia and platinum. It has also been used to coat Haynes Alloy 130 with platinum to prevent oxidation at electrical contacts. Guanidine 2-ethyl-hexanoate wets oxides as well as most metal surfaces.

This work was done by Warren H. Philipp, Martha H. Jaskowiak, and Lisa C. Veitch of Lewis Research Center, Joseph M. Savino of Cleveland State University, and Mark DeGuire of Case Western Reserve University. Further information is contained in a TSP [see page 1].

Inquiries concerning rights for the commercial use of this invention should be addressed to the Patent Counsel, Lewis Research Center [see page 1]. Refer to LEW-14984.

Micromechanics for Particulate-Reinforced Composites

Mechanical and thermal properties can be predicted faster and more easily than before.

Lewis Research Center, Cleveland, Ohio

The macroscopic mechanical and thermal properties of matrix/particle composite materials and the responses of such materials to applied loads can now be predicted by use of simplified equations derived from basic considerations of micromechanics. Typical bounding methods — and such numerical methods as finite-element analysis — provide bounds on the effective macroscopic thermal and mechanical properties of matrix/particle composites. These methods entail major disadvantages: either the bounds are far apart, or (when numerical techniques are used) the computations take too much time to be practical for frequent or routine analyses. In contrast, the simplified equations are highly computationally efficient and yield results within engineering accuracy.

The simplified equations predict the thermal and mechanical properties, averaged over volumes large enough so that the material appears homogeneous, on the basis of (1) the thermal and mechanical properties of the constituent materials and (2) such fabrication-related parameters as the sizes and volume fractions of the particles. With the help of simple microstress equations, it is also possible to predict the stress and strain in each constituent. The simplified equations are usually in closed form and, unlike the equations of older methods, do not require either numerical integration or iteration. Thus, the equations are computationally efficient yet capable of adequately modeling the applicable physics.

The derivation of the simplified equations starts from a mechanics-of-materials approach at the microscopic scale — similar to the approach followed previously with respect to matrix/fiber composite materials. The particles are modeled as being spheres of equal diameter dispersed uniformly throughout the matrix or binder material on a cubic lattice. The diameter of the modal particles is an average calculated from the distribution of sizes of the real particles. The distance between neighboring particles on the lattice is computed from the sizes and volume fraction of the particles. Each cell of the lattice is regarded as a representative volume element; the micromechanics equations are developed for this volume element and used to represent the macroscopic properties of the composite material.

The simplified equations have been tested by applying them to two materials: (1) a particulate composite with constituents that have properties representative of those of constituents of concrete, and (2) a metal-matrix/particle composite that is a candidate for use in some automotive applications. The predictions obtained from the equations were compared with bounds obtained by other methods and with experimental data, where available. The results of these tests confirmed the expectations of computational efficiency and of the excellence of the micromechanics predictions.

This work was done by Pappu L. N. Murthy and Robert K. Goldberg of Lewis Research Center and Subodh K. Mital of The University of Toledo. Further information is contained in a TSP [see page 1].

Inquiries concerning rights for the commercial use of this invention should be addressed to NASA Lewis Research Center, Commercial Technology Office, Attn: Tech Brief Patent Status, Mail Stop 7-3, 21000 Brookpark Road, Cleveland, Ohio 44135. Refer to LEW-16370.

Electrically Conductive Thermal-Control Coating Materials

The materials retain electrical conductivity during exposure to vacuum.

Marshall Space Flight Center, Alabama

Coating materials that consist largely of tin oxide exhibit a useful combination of solar absorptance, thermal emittance, and electrical conductivity. The materials are intended for use as thermal-control coats for spacecraft; they may also be useful on industrial or scientific vacuum-equipment surfaces that are required to exhibit their specific thermal-radiation and electrical properties. Unlike older materials used for the same purpose, these materials do not lose electrical conductivity during long exposure to vacuum.

A material of this type is made highly electrically conductive by incorporating antimony and indium via chlorides or oxalates in concentrations of 1 to 4 weight percent relative to the amount of tin oxide. The antimony and indium produce extrinsic defects within the crystal lattice of the tin oxide. These defects bring electrons in the valence band close enough to the conduction band to make the electrons highly mobile between the bands. This results in high electrical conductivity.

The ingredients are mixed in several steps of wet and dry ball milling. The mixture is heated to a temperature between 1,000 and 1,100 °C for four hours, then cooled, then milled again. Next, the material is mixed with a resin and solvents to form a liquid mixture that can be sprayed to coat the surface in question.

This work was done by Richard J. Mell of **Marshall Space Flight Center.** *Further information is contained in a TSP [see page 1].*

Inquiries concerning rights for the commercial use of this invention should be addressed to the Patent Counsel, Marshall Space Flight Center [see page 1]. Refer to MFS-28916.

Books and Reports

Oxidation-Barrier Coatings for Refractory Metals

A report reviews the technology of metal coatings for protecting refractory metal substrates against oxidation at high temperatures. Potential applications for this technology include gas-turbine engines, heat exchangers, furnace components, equipment for handling molten metals, thermocouples, radiation-cooled spacecraft thrusters, and high-temperature-resistant structural components. The report describes processes and procedures for depositing coatings, with emphasis on the following major achievements:

- Development of means to deposit thick platinum and rhodium coatings with lower stresses and fewer microcracks than were previously achievable;
- Development of processes to deposit thick, adherent coatings of platinum-group metals on refractory substrates, without need for intermediate coatings, such that the coatings remain bonded through high temperature excursions;
- Demonstration that useful alloys of refractory metals and platinum coatings can be formed through thermal diffusion;
- Demonstration that selected barrier coatings on refractory substrates can withstand severe oxidizing environments at temperatures from 1,260 to 1,760 °C for long times; and
- Successful application of the deposition processes and procedures to prototype hardware.

This work was done by G. A. Malone and T. Walech of Electroformed Nickel, Inc., for **Lewis Research Center.** *To obtain a copy of the report, "High Temperature Barrier Coatings for Refractory Metals," see TSP's [page 1].*

Inquiries concerning rights for the commercial use of this invention should be addressed to NASA Lewis Research Center, Commercial Technology Office, Attn: Tech Brief Patent Status, Mail Stop 7-3, 21000 Brookpark Road, Cleveland, Ohio 44135. Refer to LEW-16456.

Tests of Thermal-Barrier and Wear Coats in Rotary Engines

A report describes experiments to evaluate combination thermal-barrier/self-lubricating coating layers on the internal sliding-contact surfaces of the housings of air-cooled rotary internal-combustion engines. These coatings were described in "Combination Thermal Barrier and Wear Coatings for Engines" (LEW-15356), *NASA Tech Briefs*, Vol. 19, No. 5 (May 1995), page 62. Each combination coating includes a thermal-barrier layer of zirconia that has been plasma-sprayed onto the bare housing metal, covered with a plasma-sprayed surface layer of PS-200 (a high-temperature, self-lubricating material that comprises 80 percent chromium carbide, 10 percent silver, and 10 percent calcium fluoride/barium fluoride eutectic). In the experiments, engines were instrumented with temperature sensors at key locations and tested on a fully instrumented dynamometer. The tests demonstrated the benefits of the thermal-barrier coatings in that specific fuel consumptions of the engines with the coatings were consistently lower than those of the same engines without the coatings. The PS-200 wear coats proved to be very durable under severe test conditions.

This work was done by Paul S. Moller and Michael Weigert of Moller International for **Lewis Research Center.** *To obtain a copy of the report, "Evaluation of Thermal Barrier and PS-200 Self-Lubricating Coatings in an Air-Cooled Rotary Engine," see TSP's [page 1].*

Inquiries concerning rights for the commercial use of this invention should be addressed to NASA Lewis Research Center, Commercial Technology Office, Attn: Tech Brief Patent Status, Mail Stop 7-3, 21000 Brookpark Road, Cleveland, Ohio 44135. Refer to LEW-16512.

BLANK PAGE

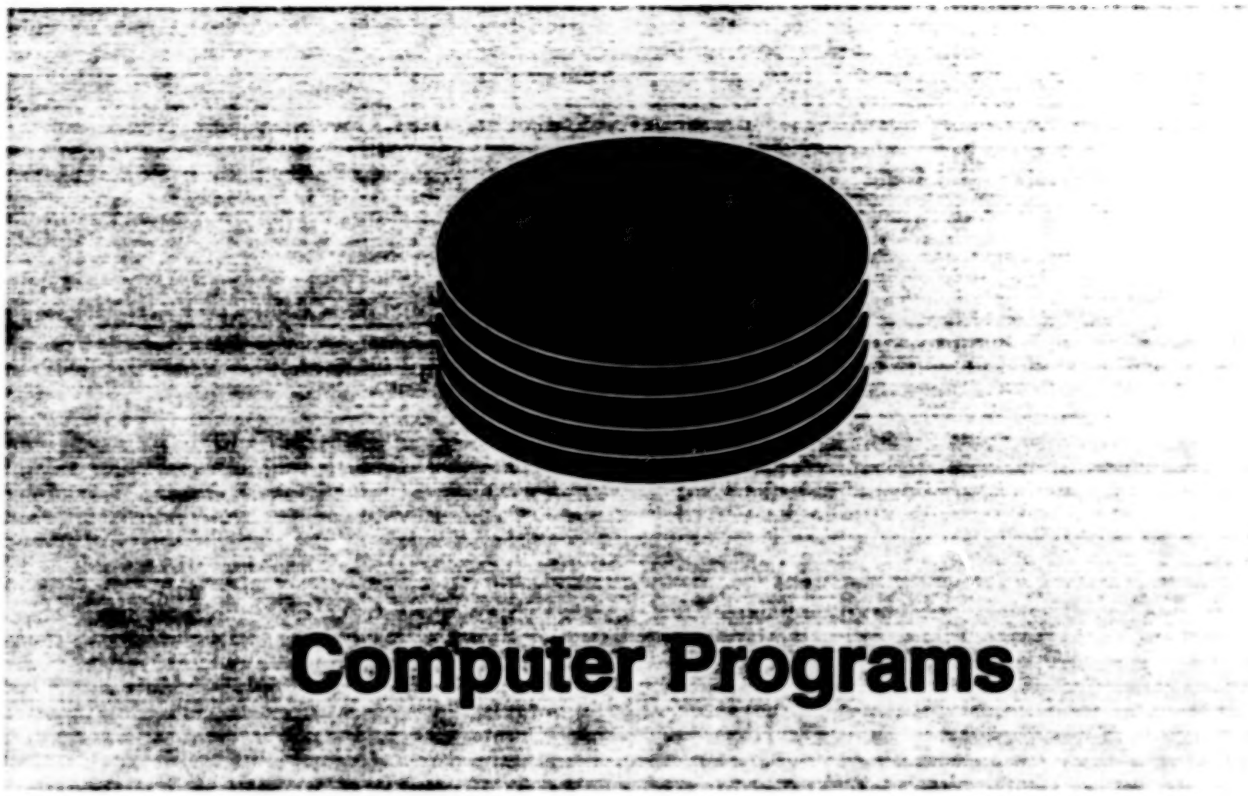

Computer Programs

Physical Sciences

Mathematics and Information Sciences

BLANK PAGE

These programs may be obtained from COSMIC. Please contact

COSMIC®
Computer Services Annex
University of Georgia
Athens, GA 30602
Telephone No. (404) 542-3265.

Physical Sciences

Software for Electrostatic Levitation

JPL+ITESL-3D is a computer program for feedback control of the three-dimensional position of an electrostatically levitated sample in an experiment on high-temperature containerless processing of the sample material. The program also acquires and displays measurements of the temperature of the sample and of the high voltages on the levitating electrodes. In JPL+ITESL-3D, tasks are allocated to foreground and background modes. In the foreground are servo-control and data-collection tasks that must be performed in real time. In the background are second-priority tasks that arise in connection with a graphical display, mouse, and keyboard. JPL+ITESL-3D runs on a Macintosh, or compatible, desktop computer and utilizes the interrupt-request capability of that computer. When an interrupt signal is issued, the computer sets aside background routines, stores the present state of its registers in memory, and launches the foreground routine. During the foreground routine, JPL+ITESL-3D receives digitized outputs of a position sensor and processes them via a proportional, integral, and derivative control law that generates a digital command for adjusting the electrode voltages to counteract any deviation of the sample from the nominal levitation position. The command is sent out through a digital-to-analog converter, and a single frame of data is collected in a specified memory buffer. After the foreground routine has been executed, the computer recaptures its previous register values and resumes its background task. This process is set into a continuous loop with an interrupt frequency of 480 Hz.

This program was written by Sang K. Chung and Won-Kyu Rhim of Caltech for NASA's Jet Propulsion Laboratory. Further information is contained in a TSP [see page 1].

This software is available for commercial licensing. Please contact Don Hart of the California Institute of Technology at (818) 393-3425. Refer to NPO-19986.

Mathematics and Information Sciences

Software Simulates Observations by a Spaceborne Camera

The SceneGen computer program simulates observational data that would be acquired by a video camera used for navigation aboard a spacecraft. SceneGen consists of two parts: a "virtual world" part that mathematically models the world that the spacecraft is expected to encounter and a camera-subsystem part that mathematically models the behavior of the camera and associated instrumentation. The virtual-world part of the software is based on physics and provides for the accurate simulation of light-path traces and photon counts. The camera-subsystem part of the software is further subdivided into a flight module and a support module. The flight module serves as part of a command-and-data-retrieval interface between the electronic circuitry of the simulated instrumentation and other subsystem modules of spacecraft flight software. The support module simulates the behavior of the camera subsystem and the generation of observational data during interactions with the virtual world.

This program was written by Maemong Lee, Ray L. Swartz, and Richard Welcher of Caltech for NASA's Jet Propulsion Laboratory. Further information is contained in a TSP [see page 1].

This software is available for commercial licensing. Please contact Don Hart of the California Institute of Technology at (818) 393-3425. Refer to NPO-20053.

Program Simulates Views From Simulated Flights Over Terrain

The Surveyor computer program generates images of terrain of the Earth and other planets as would be seen during simulated flights over the terrain. Some previously developed programs offer some of the same capabilities, but none can handle the large data sets that Surveyor can handle. Surveyor accepts elevation and surface-feature-texture data acquired by remote sensing during previous real flights over a given terrain, then processes the data to simulate the evolving view from a simulated flightpath. Surveyor provides a user interface for building simulated flightpaths; the user generates such a trajectory interactively, with the help of a real-time rendering capability that enables previewing. Once the flightpath has been generated, Surveyor generates sequential frames of data representing high-quality animation images that can be made to have various resolutions suitable for various film and video formats. Surveyor has been executed on a Silicon Graphics workstation with 256 MB of random-access memory, a 9-GB hard drive, and a 20-in. (51-cm) monitor. It can also be run on Sun workstations using the SunOS operating system.

This program was written by Zarah Gorjian, Steve Watson, Dave Kagels, Paul Asmar, Dan Stanilli, Bena Currin, and Gigi Yates of Caltech for NASA's Jet Propulsion Laboratory. No further documentation is available.

This software is available for commercial licensing. Please contact Don Hart of the California Institute of Technology at (818) 393-3425. Refer to NPO-20043.

Computer Program Generates Software From Facts and Rules

The Automatic Code Generator (ACG) is a computer program that decreases the effort and thus the cost of developing ZP-SIM software. [ZPSIM is a software system for constructing computer programs to test control software when the control computer and/or other electronic control hardware (e.g., an avionic system) is not available for testing.] The input to the ACG is a concise list of facts that must hold for the code that one seeks to develop, along with domain-specific knowledge like design rules and patterns. The application programmer writes only these facts, rather than the code. The design rules are provided by system architects. The ACG comprises two components: (1) a specification compiler, which translates specifications into facts for an inference engine and (2) the inference

engine, which synthesizes C++ code from the facts and rules. The inference engine is based on the CLIPS expert-system software. The ACG is in daily use, supporting the development of mission-critical software within the ZIPSIM project. The increment of productivity afforded by the ACG is approximately equivalent to that of one human programmer.

This program was written by William K. Reinholtz of Caltech for NASA's Jet Propulsion Laboratory. Further information is contained in a TSP [see page 1].

This software is available for commercial licensing. Please contact Don Hart of the California Institute of Technology at (818) 393-3425. Refer to NPO-19981.

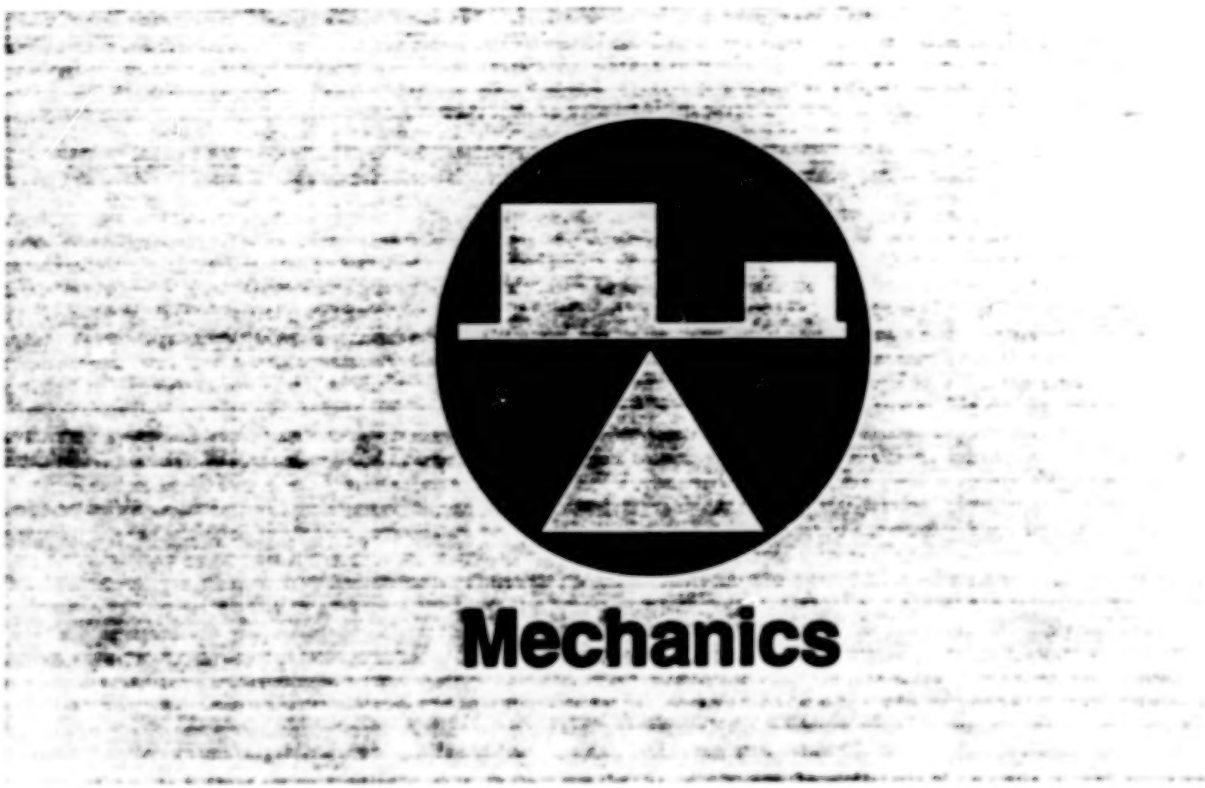

Mechanics

Hardware, Techniques, and Processes

BLANK PAGE

Valve Meters Hot, Pressurized Oxygen

The design minimizes upstream disturbances and obstructions to flow.

Lyndon B. Johnson Space Center, Houston, Texas

The figure illustrates a valve, similar to a ball valve, that meters a flow of oxygen at temperatures up to 500 °F (260 °C) and pressures up to 10,000 psi (about 7 MPa). The valve is designed to minimize the pressure drop and the concomitant upstream-propagating pressure disturbances, and to keep the speed of flow nearly constant. Accordingly, the valve is configured not to restrict the flow but to direct all or part of it to a primary outlet (in which the metered flow is required) or to a secondary outlet (which could be connected to a return or recirculation tube).

The valve body, the shaft, and the valve member (which is machined integrally with the shaft) can be made of stainless steel(s) and/or suitable nickel alloy(s). The flow path is kept as straight as possible to minimize both turbulence and the cross sections presented by corners and other obstructions on which particles entrained in the flow can impinge. This latter feature is particularly important because particles and valve surfaces are heated upon impact, and the particles are particularly susceptible to ignition in hot, pressurized oxygen.

The valve member is a cylinder (instead of a sphere as in a ball valve). It contains a single, straight flow passage of oval cross section that tapers to an enlarged opening at the inlet end. The opening in the valve member at its outlet end is large enough to straddle a wedge in the valve body that divides the flow into two parts, each going to one of the outlets. Thus, depending on the shaft angle, all or part of the flow can be directed to either or both outlet(s). The wedge divides the flow with minimal disruption of the flow and minimal back pressure, and presents a small cross section to oncoming particles.

The valve member turns in a closely fitting tubular sleeve in the valve body. Seals between the shaft and the valve body are formed by frustoconical seal rings made of a copper alloy or other deformable material. The seal rings are sandwiched between backup rings (which are basically thick washers) and squeezed axially against the tubular sleeve by use of packing nuts. The resultant wedging of the seal rings against each other forces the rings tightly against the shaft and valve body. Despite the tight seal, the frictional torque is relatively low, and the shaft can be turned easily; this is important because it enables the valve-actuating mechanism to adjust the valve quickly and accurately to the specified flow settings.

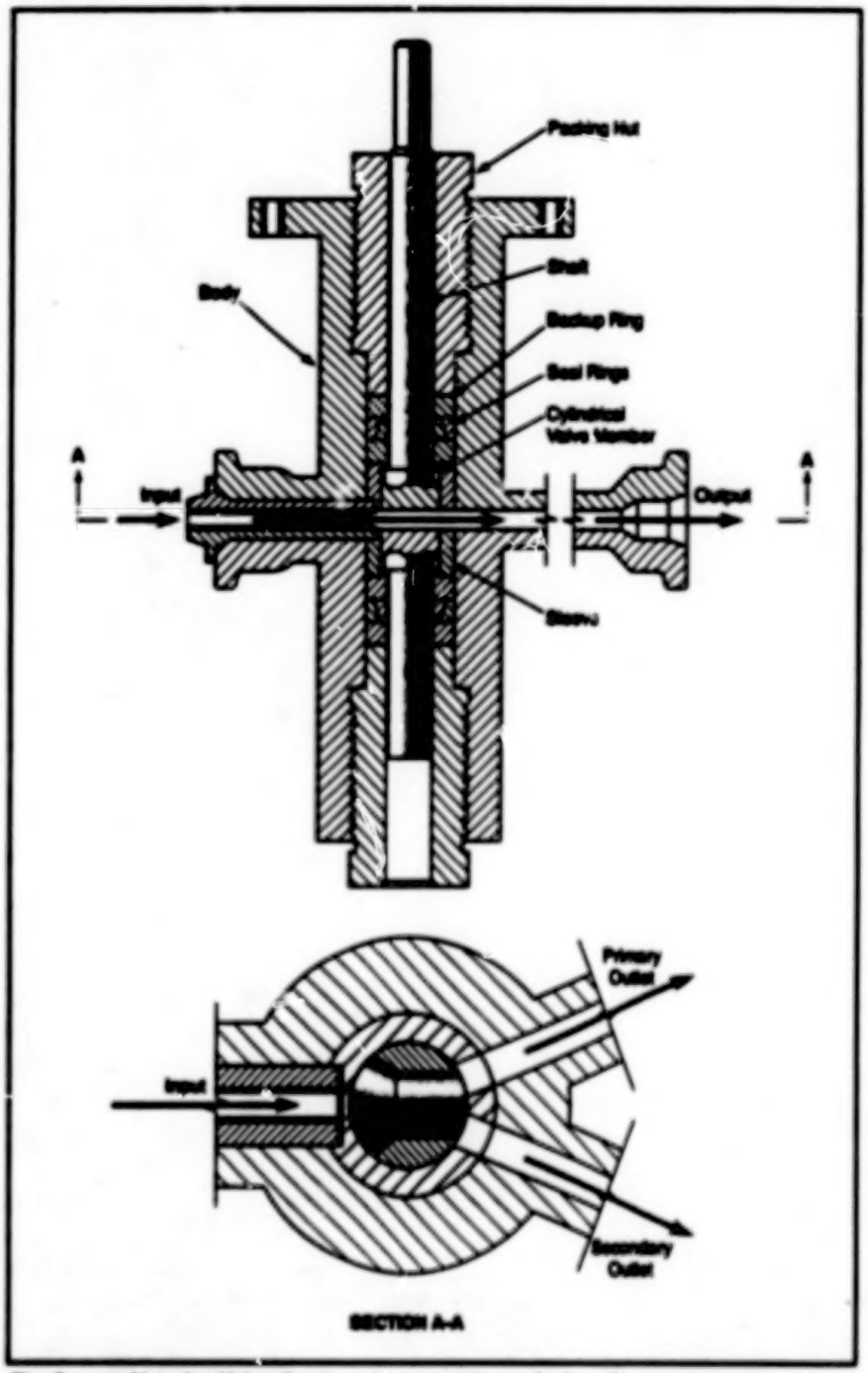

The Oxygen-Metering Valve directs various proportions of a flow of hot, pressurized oxygen to the primary and secondary outlets.

This work was done by Rollin C. Christenson, James A. Daniel, and Peter P. Lycou of Lockheed Engineering & Sciences Co. for Johnson Space Center. Further information is contained in a TSP [see page 1].

This invention has been patented by NASA (U.S. Patent No. 5,251,663). Inquiries concerning nonexclusive or exclusive license for its commercial development should be addressed to the Patent Counsel, Johnson Space Center [see page 1]. Refer to MSC-21823.

Calibrating Aircraft-Vibration Models From Flight Data

These models can be used in flight simulations and analyses of handling qualities.

Dryden Flight Research Center, Edwards, California

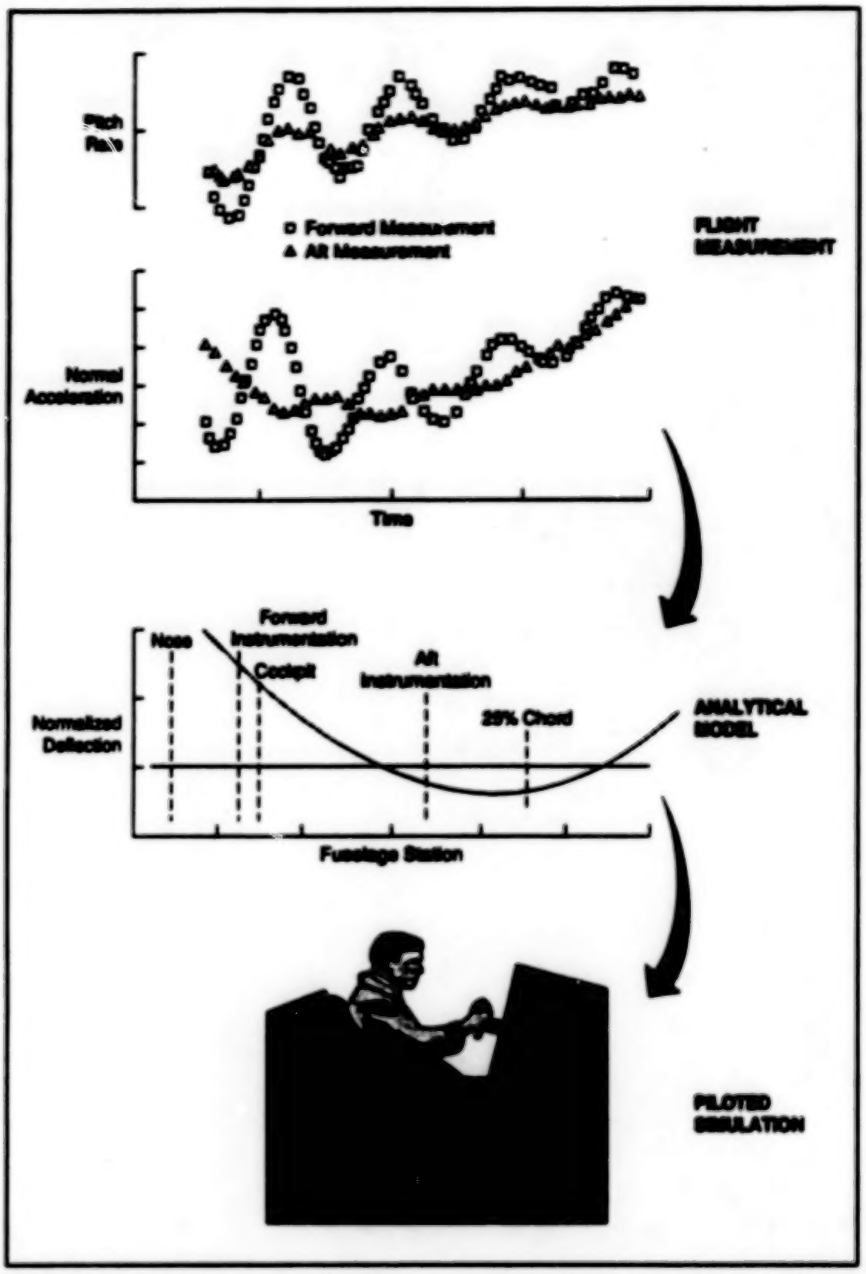

Pitch-Rate and Normal-Acceleration Data acquired by minimal instrumentation in minimal flight can be processed into mode-shape information with minimal analysis.

A methodology for constructing mathematical models of vibrations of aircraft has been developed with a view toward using such models in piloted flight simulations and in computational analyses of handling qualities of aircraft. The methodology provides for the extraction, from flight data, of vibrational-mode-shape information comparable to the information obtainable in a ground-based vibration test or in a detailed computational analysis of the dynamics of an aircraft structure. A computer program that implements a model developed according to this methodology can then be incorporated into the flight-simulation computer program for the aircraft to obtain a good representation of flight characteristics for analyses of aircraft handling qualities and of the performances of aircraft control systems.

Performance requirements for advanced aircraft and aerospace vehicles generally give rise to design requirements for structures as lightweight as possible. For advanced cruise aerospace vehicles (e.g., the High Speed Civil Transport) and for single-stage-to-orbit aerospace vehicles, requirements for maneuvering are quite low and gross weights are high. As a result, structures are relatively flexible and frequencies of vibrational modes approach the frequencies characteristic of the rigid-body dynamics of the vehicles. It therefore becomes necessary to include the vibrational modes in analyses of control systems and handling qualities of the vehicles. The mathematical model used to simulate the vibrations and other relevant aspects of the dynamics of a vehicle must be modified further to reduce the model to one that is applicable to the frequency ranges of significance to the pilot.

Often in flight-test programs, the available mathematical models of structural dynamics do not correspond exactly to the aircraft structures in question. Data from conventional ground-based vibration tests can be used to update these models, but such tests are expensive and time-consuming and are rarely performed to support handling-qualities flight experiments.

The present methodology enables the construction of suitably reduced models from flight data in a fraction of the time and at a fraction of the cost of acquiring and processing data from ground-based vibration tests. This methodology was developed and demonstrated in conjunction with the NASA SR-71 handling-qualities flight-test program. Data obtained throughout the ranges of velocities and altitudes of the SR-71 airplane were processed to extract the characteristics of the first vibrational mode that involves bending of the longitudinal axis of the airplane. These characteristics have been incorporated into mathematical models that have, in turn, been incorporated into computer programs for piloted and batch flight simulations that will support analyses for the handling-qualities flight-test program.

The methodology provides for calibration of a simplified mathematical model of those modes of vibration of the aircraft structure that are of significance for piloted simulations. For the SR-71 airplane,

the first longitudinal-axis-bending mode is the vibrational mode of greatest significance. This mode is represented by a second-order submodel, and modes of higher order are modeled by use of a delay. The modal responses at various fuselage locations are obtained from the distribution of such responses for a uniform-beam submodel that can be calibrated from flight data. More specifically, pitch-rate and normal-acceleration data (see figure) from at least two locations are needed to calibrate the solution for the uniform-beam submodel.

Mode shapes obtained by following this approach have been compared with mode shapes obtained from ground-based vibration tests, and the general form of the uniform-beam solution was found to be a good representation of the mode shapes in areas of interest. A technique of manual analysis and calibration has been developed and is applicable to the case in which the structural dynamic (vibrational) motion is not altered significantly by the aircraft control system. A parameter-estimation technique has been developed for the more difficult case in which there is a control-system interaction or a short-period interaction prevents a simple analysis; this technique can be implemented by use of standard parameter-estimation programs or by use of personal-computer spreadsheet analysis programs with equation-solving capabilities.

This work was done by Bruce G. Powers of Analytical Services and Materials, Inc., for **Dryden Flight Research Center.** *Further information is contained in a TSP [see page 1].*
DRC-95005

Single-Event, Low-Rebound Energy Absorber

Kinetic energy would be dissipated in cutting a solid material.

NASA's Jet Propulsion Laboratory, Pasadena, California

Single-event, low-rebound dampers have been invented to cushion spacecraft during planned landings on other planets and asteroids. Similar damping mechanisms might prove useful on Earth for protecting passengers and cargoes involved in aircraft and land-vehicle crashes.

Typical damping mechanisms designed for one-time use utilize a crushable or deformable element to absorb impact energy. While this method is capable of significantly reducing impact energy, it stores some energy elastically in the crushed or deformed material, which is then returned to the system as a rebound force.

This damping mechanism absorbs energy by shearing material instead of crushing material. Energy is still stored elastically in the material, but it is not returned to the system as a rebound force.

The mechanism superficially resembles an automotive shock absorber in that it includes a tube sliding within a slightly wider tube (see figure). The inner tube is filled with a polyurethane foam. A cutting-and-coring assembly is mounted on the end of a hollow shaft within the outer tube and is partially embedded into the foam.

Pushing the two ends of the damper inward causes blades on the cutting-and-coring assembly to cut into the foam. Once the blades have penetrated to their full length, the cutting stroking force becomes constant, and so the energy dissipated in cutting the foam depends mainly on the length of the stroke. Because most of the energy is not spent in compressing the foam axially, there is little potential energy left to cause rebound once the stroking force is removed.

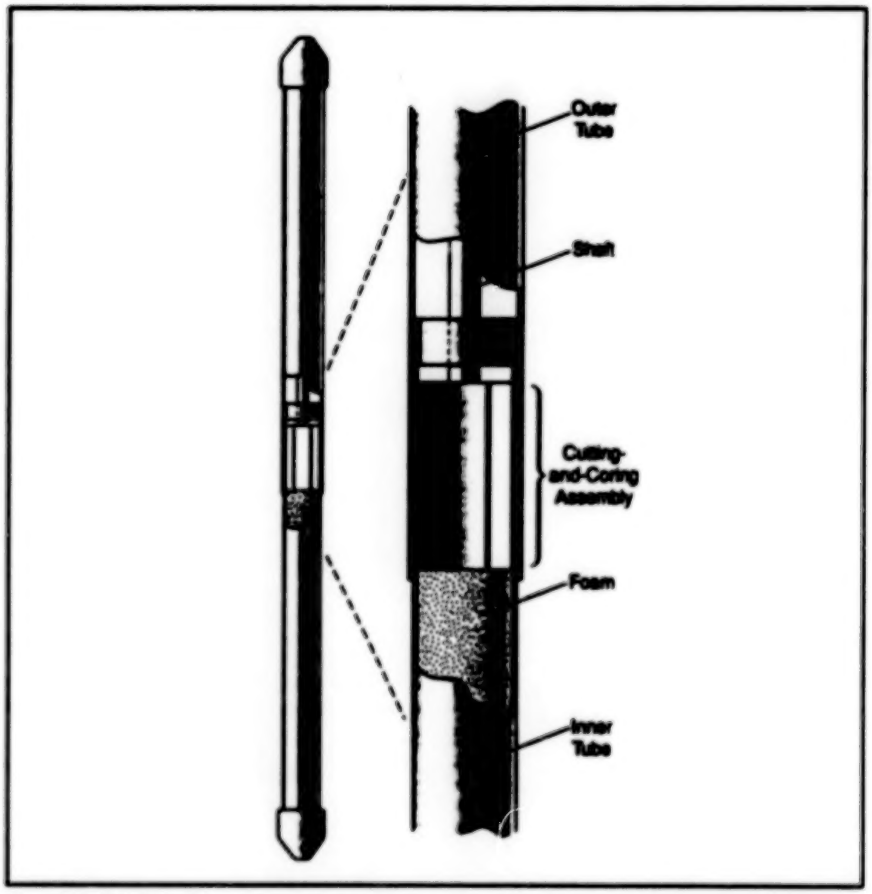

Energy Is Dissipated in cutting the foam when the ends of the tubes are pushed toward each other.

This work was done by Kevin Burke, Greg Gillis-Smith, Doug Henderson, Randel Lindemann, and Richard Rainen of Caltech for **NASA's Jet Propulsion Laboratory.** *No further documentation is available.*
NPO-20102

Estimating Repair-Weld Strengths Using Wide-Panel Specimens

Wide-panel specimens give better approximations of realistic stress patterns.

Marshall Space Flight Center, Alabama

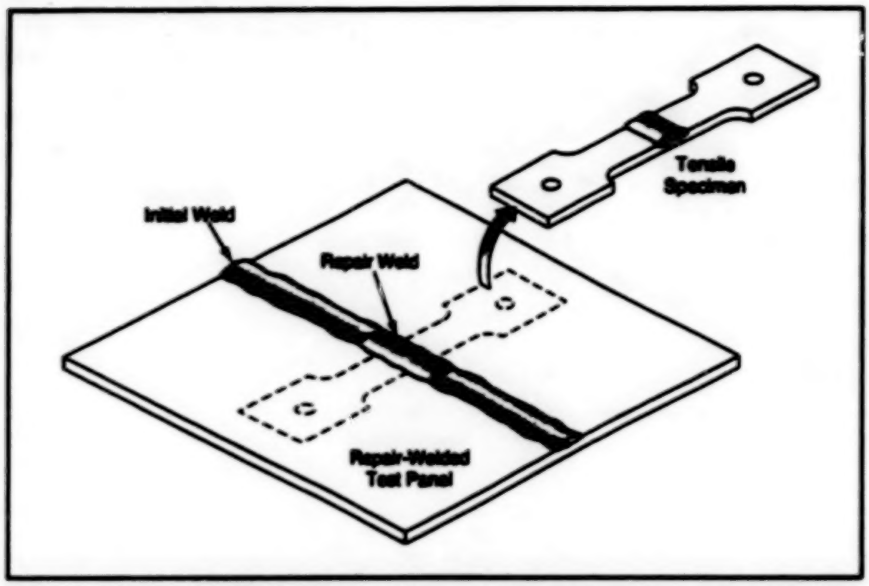

Figure 1. A Narrow Tensile Specimen cut from part of the repair weld in a repair-welded test panel yields incomplete information because it does not incorporate the effects of the surrounding panel material.

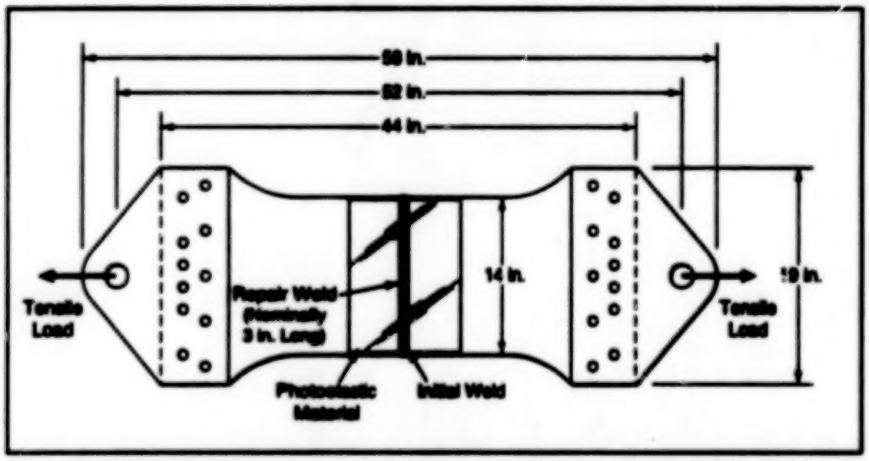

Figure 2. A Wide-Panel Specimen is a repair-welded test panel that contains both a repair weld and a substantial amount of surrounding material, as would typically be found in a practical repair-welded structure. In this case, the specimen includes clevis plates to facilitate tensile testing. The dimensions shown here are typical only.

A technique for determining the effect of a repair weld upon the strength of a previously welded workpiece involves tensile testing of a wide-panel specimen that is coated with photoelastic material to reveal strains. (As used here, "repair weld" denotes a portion of an initial weld that has been rewelded to remove a defect.) The technique provides for assessment of the effects of residual stresses that the repair weld introduces into the surrounding workpiece material, including the nearby portions of the initial weld not included in the repair weld. The invention has been used to assess the effects of residual stresses, degradation of strengths, and redistribution of loads in 2195 aluminum/lithium alloy repair welds in the Space Shuttle Super Lightweight External Tank program. The technique could easily be adapted to assessment of these effects in high-performance welded structures in other applications.

Heretofore, it has been common practice to cut relatively narrow [up to 2-in. (5-cm) wide] tensile specimens from a repair-welded test panel (see Figure 1), then test these specimens to failure to determine the strengths of the initial and repair welds. The major disadvantage of the narrow-specimen technique is that it cannot capture (1) the effects of residual stresses introduced by a repair weld and (2) redistribution of loads in a structure that contains a repair weld. This is because removing a narrow specimen (1) removes the constraint of surrounding material, which is the source of residual stresses and (2) removes any capability for sharing and redistribution of load in the surrounding material.

The present wide-panel testing technique is designed to capture the combined effects of residual stresses, degradation of strength, and redistribution of load around a repair weld. A wide-panel specimen represents a repair weld more closely than does a narrow tensile specimen because it is a welded test panel that contains the full length of a repair weld within a longer initial weld.

Figure 2 illustrates a typical wide specimen. After the specimen has been fabricated by welding and machining, a commercially available photoelastic material is bonded to it in the weld area. The specimen is then tensile tested. With the help of polarizing optical filters, the strains produced by the tensile test can be observed as a colored fringe pattern. Through this technique, differences among various repair welds and weld-material/parent-material combinations can be observed. The strain patterns made visible by the photoelastic material can also be compared and correlated with strain patterns predicted by finite-element structural-analysis computer programs.

This work was done by Patrick R. Rogers and Julian E. Bynum of Marshall Space Flight Center. Further information is contained in a TSP [see page 1].
MFS-31106

Modified Tether-Hook Mechanism With Locking Lever

A tether-hook mechanism that was previously somewhat difficult to unlock and release by hand has been modified to enable release by natural-feeling placement of a hand on the hook and simple squeezing. Incorporation of a lever operated by the hand to unlock the ball of the hook eliminates the cumbersome requirement, in the previous design, to align the index finger and thumb on corresponding locks in order to release the hook. The modified tether-hook design could be useful in such safety-hook applications as construction, window washing, and underwater operations that require a self-locking tether hook that is easy to operate.

This work was done by Robert C. Trevino of **Johnson Space Center**. *Further information is contained in a TSP [see page 1].*
MSC-22593

BLANK PAGE

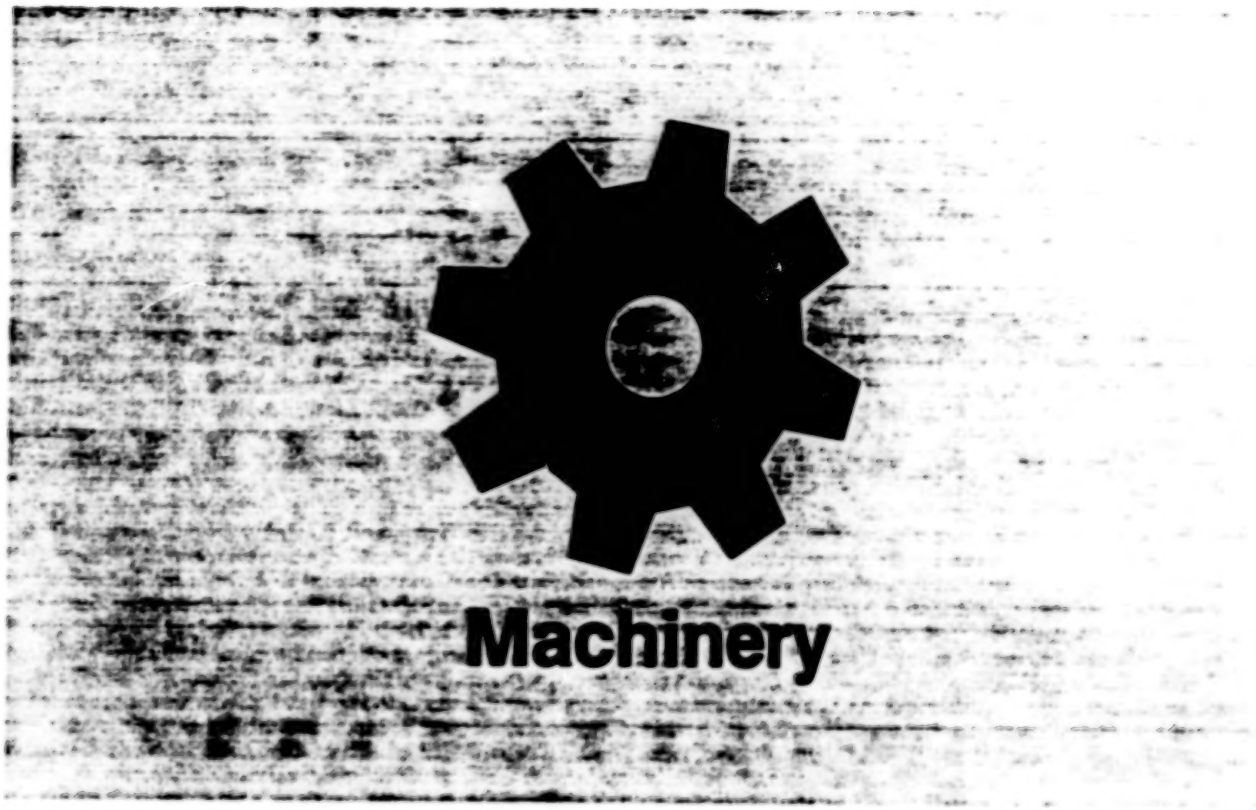

Machinery

Hardware, Techniques, and Processes

48

BLANK PAGE

Thermoacoustic Refrigerator

Inert gases are used as working fluids in place of potentially harmful CFCs, HFCs, or HCFCs.

Lyndon B. Johnson Space Center, Houston, Texas

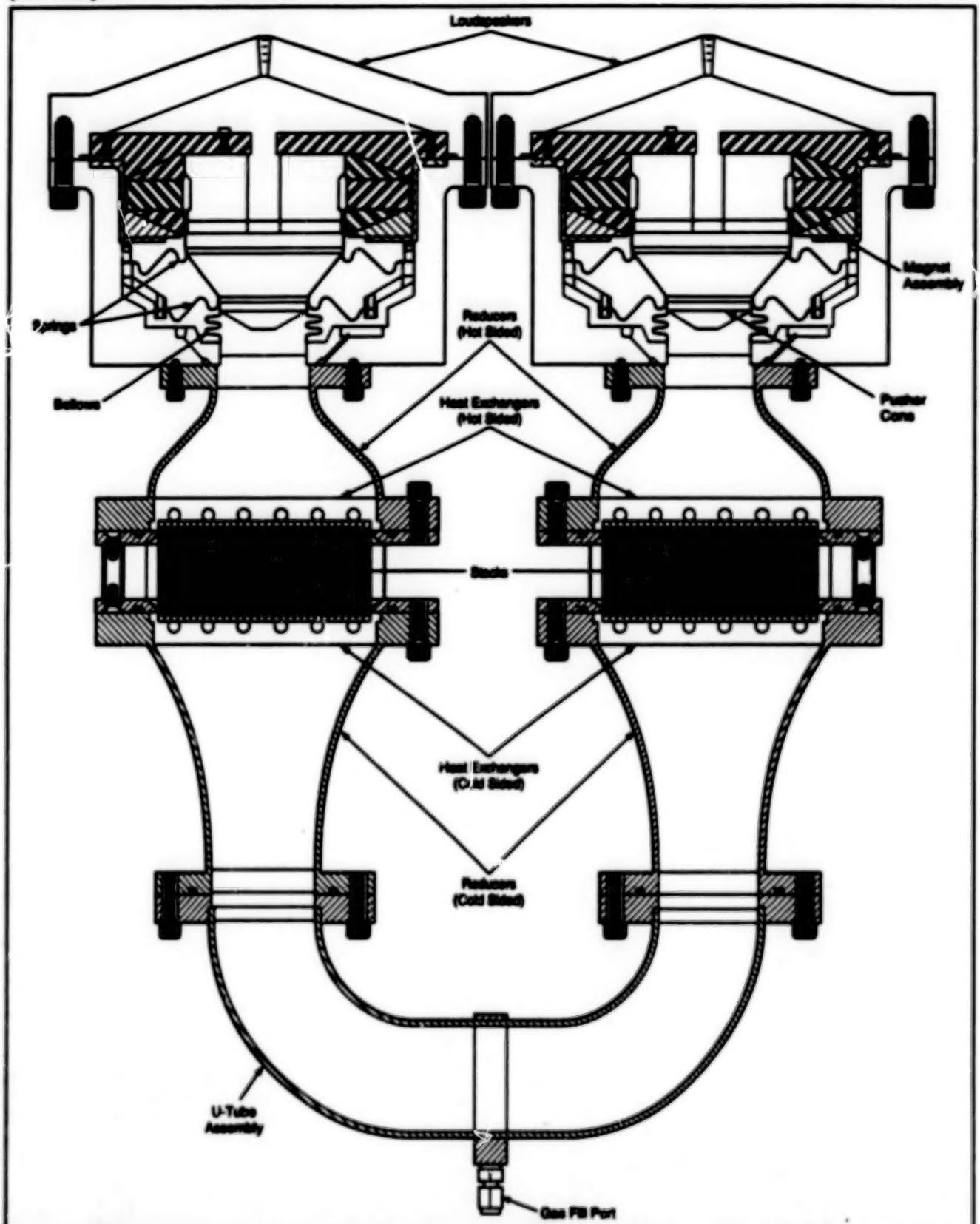

The Two Loudspeakers Maintain a Half-Wavelength Standing Wave at a resonant frequency of 320 Hz in a 20 atm. mixture of helium and argon gas. The two stacks are 11-cm-diameter spirals of 52-μm-thick plastic with a spacing of 204 μm. At either end of each stack are finned heat exchangers attached to tubing which allows the heat-transport fluids to deliver useful cooling to the refrigerated enclosure and to exhaust the waste heat plus work.

A thermoacoustic refrigerator produces high-amplitude sound waves in an inert gas mixture to pump heat without using chlorofluorocarbons (CFCs), which are dangerous when leaked into an enclosed environment. Chemical refrigerants such as CFCs and HCFCs are also known to destroy stratospheric ozone and, along with HFCs, are "greenhouse" gases which contribute to global warming.

Two electrodynamic loudspeakers, each capable of generating 100 W of acoustic power, operate at a frequency of 320 Hz to establish a standing wave in the mixture of helium and argon gas at a static pressure of 20 atm. This sound wave causes compressions and expansions of the gas which are accompanied by oscillatory gas motion. The compressions and expansions raise and lower the temperature of the gas. Within the "stack" section of the refrigerator, these oscillating gas parcels can pick up heat from the stack and deposit heat to the stack at a different location. These gas parcels therefore act like a "bucket brigade" which removes heat from the cold heat exchanger and deposits it at the hot heat exchanger. Heat transfer fluids are pumped through the hot and cold heat exchangers to deliver useful cooling to an insulated sample enclosure and exhaust the waste heat plus work to the surroundings. The thermoacoustic device shown in the figure was designed to provide 700 Btu/h (205 W) of cooling at +4 °C and 400 Btu/h (117 W) of cooling at –22 °C with an exhaust temperature of +20 °C. In recent sea trials onboard the *USS Dayo* (DD-969), 1430 Btu/h (419 W) of useful heat load was removed from shipboard radar electronics while the destroyer was underway near Annapolis, MD.

This work was done by Steven Garrett of Sound Advice Acoustical Consulting for **Johnson Space Center**. *Further information is contained in a TSP [see page 1].*

In accordance with Public Law 96-517, the contractor has elected to retain title to this invention. Inquiries concerning rights for its commercial use should be addressed to

Donald Lincoln
Patent Counsel (Code 006)
Naval Postgraduate School
Monterey, CA 93943
(408) 656-2506

Refer to MSC-22064, volume and number of this NASA Tech Briefs *issue, and the page number.*

Acoustic-Emission Bearing-Fault Diagnostics System

Analytical software differentiates between bearing failure and transient-event signals during testing of turbomachinery and drive-train systems.

Marshall Space Flight Center, Alabama

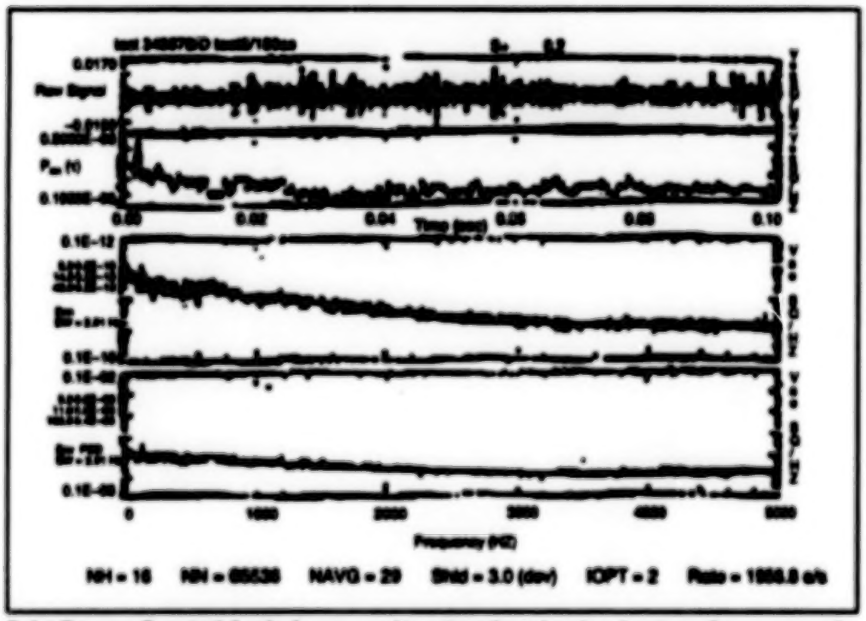

Point-Process Spectral Analysis was used to extract these bearing signatures from an acoustic emissions transient signal during testing of a good bearing.

A new hardware and software system that uses a state-of-the-art, high-frequency Acoustic Emissions (AE) sensor and an innovative AE signal-processing technique, called Point Process Spectral Analysis (PPSA), has been developed to help prevent catastrophic failures and costly down time due to false alarms during bearing testing. In the past, bearing health monitoring and fault diagnosis within turbomachinery and drive-train systems have been a significant technical challenge for the aeronautics and transportation industries.

Previous techniques to detect bearing faults could not distinguish between transient events related to shaft rotational processes and the signatures associated with defective bearings. Also, these techniques did not involve high-frequency, real-time analysis. To overcome these unique problems, PPSA was developed to meet the high-frequency AE signal processing and fault detection requirements.

Conventional time series representation of an ultra-high frequency AE signal requires all data to be sampled over the entire waveform at a high sampling rate. However, PPSA only uses the times occurrence of the transient events, along with their strengths, since these transient events contain the major dynamic information needed for bearing fault detection. As a result, PPSA requires much less data to analyze the frequency-domain behavior than conventional time-series representation. Additionally, PPSA overcomes the basic limitations of the fast-Fourier- transform-based spectrum for detecting signal components, such as widely spaced, narrow transient spikes that cannot be approximated effectively by a sum of sinusoids.

PPSA uses the first moment function of time to determine the rate of transient impulses, thresholding the temporal AE waveforms for structural failure detection. Next, a mean-lag-jump product, representing the second moment of a point process, provides a statistical estimation of the correlation between all pairs of event occurrences with common time lags. The frequency-domain representation of the second-moment mean-lag-jump product function is used to create a spectrumlike function of the point-process. This point-process spectrum provides a statistical estimation of the event occurrence rate and intensity distribution as a function of frequency.

The superior detection capability of PPSA over conventional envelope analy-

sis in extracting bearing signatures from AE transient signal in a noisy operational environment was demonstrated with two computer-simulation examples and with NASA-provided test data from a bearing test rig. Three test conditions were used: a good bearing, an inner race defect, and a roller defect. PPSA successfully analyzed the data. The results of these proof-of-concept studies indicated that PPSA can provide high computational efficiency in processing ultrahigh-frequency AE signals and is highly suitable for real-time implementation. Using this analysis technique would significantly reduce the digital signal processor requirement in developing a low-cost, commercially viable, on-line bearing-diagnostic system.

This work was done by Jen-Yi Jong of AI Signal Research, Inc., for the Marshall Space Flight Center. Further information is contained in a TSP [see page 1].
MFS-26468

BLANK PAGE

Mathematics and Information Sciences

Books and Reports

BLANK PAGE

Books and Reports

Autonomous Navigation for Spacecraft Orbiting Earth

A report proposes a method of autonomous navigation of spacecraft in orbit around the Earth. The method, to be implemented by use of on-board computers and on-board Global Positioning System (GPS) receivers, would be applicable to a single spacecraft or to multiple spacecraft flying in formation as needed for some coordinated scientific observations. Simple empirical quadratic fits to ground-track offsets would be computed from orbits as determined kinematically in real time by use of the GPS data. No atmospheric-drag predictions would be necessary, inasmuch as the drag information would be inferred from the quadratic fits. The quadratic fits would also be used to predict the times and sizes of future maneuvers that would be necessary to satisfy such navigational requirements as repeating specified ground tracks and/or flying in formation at specified separations. The main benefit of the method would be elimination of the need for ground operators to determine command sequences for orbit-adjustment and -maintenance maneuvers.

This work was done by Joseph Guinn, Mark Vincent, and Ronald Bosh of Caltech for NASA's Jet Propulsion Laboratory. To obtain a copy of the report, "Spacecraft Autonomous Navigation for Formation Flying Earth Orbiters Using GPS," see TSP's [page 1].
NPO-20116

Robust Numerical-Integration Schemes for Viscoplasticity

A report discusses the development of a general conceptual framework for implicit time-stepping numerical-integration schemes used to solve the equations of flow and of evolution of materials in generalized mathematical models of viscoplasticity. The general theoretical aspect of the framework is developed, starting from the unconditionally stable, backward-Euler difference scheme. The mathematical structure of this framework is sufficiently general to provide unified treatment of different classes of models of viscoplasticity with internal variables. Two such models that are representative of the state of the art in viscoplasticity of metals are considered in example applications to two metals. One of these models is of the associative generalized viscoplasticity with potential structure (GVPS) type; the other model is of the non-associative (NAV) type. The matrix forms for these models are directly applicable to both initially isotropic and anisotropic materials in three-dimensional situations as well as in subspace situations (for example, situations that involve plane stress/strain, axisymmetry, or generalized plane stresses in shells). Regarding the computational aspect of the framework, issues of efficiency and robustness are emphasized in developing a local iterative numerical-integration algorithm. Significant robustness is introduced by complementing a basic Newton-Raphson scheme with a line-search strategy for convergence.

This work was done by Wei Li and Atef F. Saleeb of the University of Akron for Lewis Research Center. To obtain a copy of the report, "Robust Integration Schemes for Generalized Viscoplasticity With Internal-State Variables," see TSP's [page 1].

Inquiries concerning rights for the commercial use of this invention should be addressed to NASA Lewis Research Center, Commercial Technology Office, Attn: Tech Brief Patent Status, Mail Stop 7-3, 21000 Brookpark Road, Cleveland, Ohio 44135. Refer to LEW-16513.

BLANK PAGE

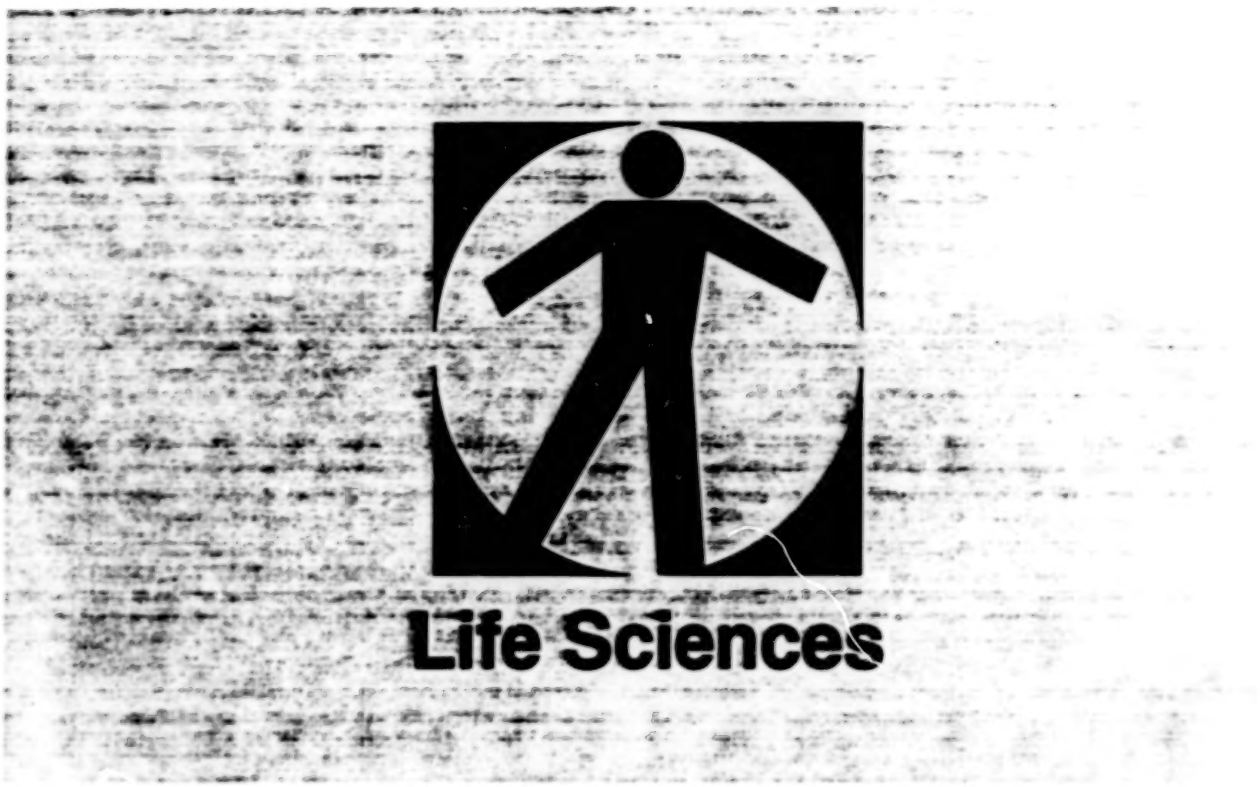

Hardware, Techniques, and Processes

BLANK PAGE

Biometric Instrument Measuring Neuromuscular Disorder/Performance Degradation

Novel "neuromuscular thermometer" gives researchers insight into fine neuromuscular control in humans.

Marshall Space Flight Center, Alabama

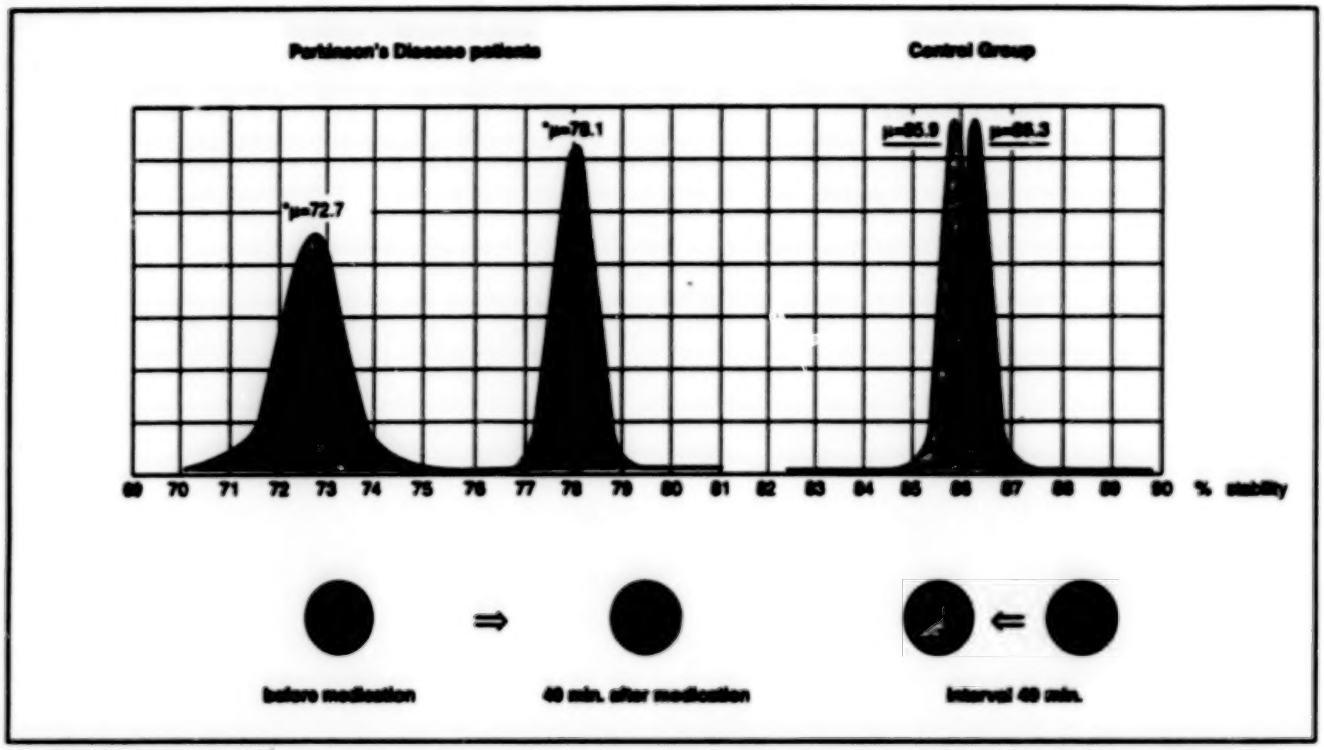

The Biometric Instrument is capable of measuring changes in fine neuromuscular control levels of patients with Parkinson's Disease.

A new device to gather quantitative information about fine neuromuscular control in humans measures deterioration of stability, smoothness, and synchronization of handwriting movements.

This device, the Neuroskill, is an ordinary-sized instrumental pen (with accompanying software), attached to a parallel port of a personal computer. The motor-sensing electronics of the Neuroskill pen has accelerometers that measure motions along the X and Y axes. It also has a pressure transducer that measures dynamics along the Z axis. The pen is easily connected to a PC by a flexible cable, such as a parallel connector normally used for a printer. Installation of the Neuroskill pen is as easy as adding a mouse to a personal computer.

Using the Neuroskill pen, the individual being tested simply writes on any surface, including regular paper. The writing may be a signature, any sequence of cursive writing, or drawn symbols.

To accurately and effectively analyze an individual's motor skill control level, designers of the Neuroskill system focused on *how the person* writes, as opposed to *how the writing looks*. The Neuroskill pen translates the written dynamics of accelerations and pressure into complex signals, each represented by 1000 data points.

Patients with Parkinson's Disease and volunteers in alcohol impairment experiments were tested with the Neuroskill device at the Colorado Neurological Institute and the Alcohol Research Center at the University of Colorado, Denver, respectively. The medical experts supervising these experiments concluded through the test results that the Neuroskill system can precisely measure the results of neuromuscular actions initiated from either the cerebellum area of the brain (where often repeated motions are controlled) or the cerebral cortex (where new tasks are believed to be controlled). The results of experiments with Parkinson's Disease patients are represented in the figure below.

Analysis of activities such as signing a signature or reproducing different cursive symbols can help the clinician to reveal the degree of damage or healing of specific parts of the brain, nerve, or muscle tissue.

With the Neuroskill device, current levels of motor skill control can be compared with previously stored results, allowing the researcher to follow the changes in motor skill control over time and choose the most effective treatment. The device also has the potential to be used as a tool in the development of neuromuscular targeted pharmaceuticals by providing real time, quantified data for use in clinical trials.

The Neuroskill device is inexpensive, non-invasive, and easy to use. The researcher or practitioner can administer the test in the work area. Additionally, the patient can continue to monitor his own condition at home between medical visits.

This work was done by Dr. Ruth Shraiman and Alexander Landau of VenFax Corporation for Marshall Space Flight Center. Further information is contained in a TSP [see page 1].

MFS-26449

END

04